NEOPLASIA
www.neoplasia.com

Volume 15 Number 8 August 2013 pp. 925–938 925

Circulating Fibronectin Controls Tumor Growth[1,2]

Anja von Au[*,†], Matthaeus Vasel[*,†], Sabrina Kraft[*,†], Carla Sens[*,†], Norman Hackl[*,†], Alexander Marx[‡], Philipp Stroebel[‡], Jörg Hennenlotter[§], Tilman Todenhöfer[§], Arnulf Stenzl[§], Sarah Schott[¶], Hans-Peter Sinn[#], Antoinette Wetterwald[**], Justo Lorenzo Bermejo[††], Marco G. Cecchini[**] and Inaam A. Nakchbandi[*,†]

*Max Planck Institute of Biochemistry, Martinsried, Germany; [†]Institute of Immunology, University of Heidelberg, Heidelberg, Germany; [‡]Department of Pathology, University Medical Center Mannheim, University of Heidelberg, Mannheim, Germany; [§]Department of Urology, University of Tübingen, Tübingen, Germany; [¶]Department of Gynecology, University of Heidelberg, Heidelberg, Germany; [#]Department of Pathology, University of Heidelberg, Heidelberg, Germany; **Department of Urology, University of Bern, Bern, Switzerland; [††]Institute of Medical Biometry and Informatics, University of Heidelberg, Heidelberg, Germany

Abstract

Fibronectin is ubiquitously expressed in the extracellular matrix, and experimental evidence has shown that it modulates blood vessel formation. The relative contribution of local and circulating fibronectin to blood vessel formation *in vivo* remains unknown despite evidence for unexpected roles of circulating fibronectin in various diseases. Using transgenic mouse models, we established that circulating fibronectin facilitates the growth of bone metastases by enhancing blood vessel formation and maturation. This effect is more relevant than that of fibronectin produced by endothelial cells and pericytes, which only exert a small additive effect on vessel maturation. Circulating fibronectin enhances its local production in tumors through a positive feedback loop and increases the amount of vascular endothelial growth factor (VEGF) retained in the matrix. Both fibronectin and VEGF then cooperate to stimulate blood vessel formation. Fibronectin content in the tumor correlates with the number of blood vessels and tumor growth in the mouse models. Consistent with these results, examination of three separate arrays from patients with breast and prostate cancers revealed that a high staining intensity for fibronectin in tumors is associated with increased mortality. These results establish that circulating fibronectin modulates blood vessel formation and tumor growth by modifying the amount of and the response to VEGF. Furthermore, determination of the fibronectin content can serve as a prognostic biomarker for breast and prostate cancers and possibly other cancers.

Neoplasia (2013) 15, 925–938

Address all correspondence to: Inaam A. Nakchbandi, MD, FACP, Professor of Medicine, Max Planck Institute of Biochemistry and University of Heidelberg, Im Neuenheimer Feld 305, 2. OG, 69120 Heidelberg, Germany. E-mail: inaam.nakchbandi@immu.uni-heidelberg.de

[1]This work was supported by the Max Planck Society (A.V.A., M.V., S.K., C.S., N.H., and I.A.N.) and the University of Heidelberg (A.V.A., M.V., S.K., C.S., N.H., and I.A.N.). No conflicts of interest exist for any of the authors.

[2]This article refers to supplementary materials, which are designated by Figures W1 to W8 and are available online at www.neoplasia.com.

Received 2 April 2013; Revised 21 May 2013; Accepted 23 May 2013

DOI 10.1593/neo.13762

Introduction

Recent studies have highlighted the key role of the extracellular matrix in tumor formation by demonstrating that changes in matrix protein concentrations or matrix composition affect tumor progression [1,2]. In the light of these results, we have investigated the function of fibronectin in this context. Fibronectin is a component of the extracellular matrix and exerts multiple effects *in vitro* and *in vivo* including stimulation of cell proliferation, migration, differentiation, and survival [3–6]. It affects cell behavior through activation of various cell surface receptors most notably integrins [7]. Fibronectin is required for the development of fibrillar structures [8] and for the storage and activation of various growth factors [9]. Recent studies of circulating fibronectin have uncovered diverse functions ranging from promotion of tumor cell invasion to bone matrix integrity and to improved recovery after brain ischemia. These studies have raised awareness of the multitude of fibronectin functions [5,10,11].

Breast and prostate cancer cells migrate away from their origin through the circulation and find a new home in the bone marrow [12,13] and eventually develop bone metastatic lesions [14]. Clinical data confirm a correlation between the presence of breast or prostate cancer cells in the bone marrow and the development of bone metastases [12,13]. There are no studies examining the role of fibronectin in the bone marrow despite evidence that fibronectin is upregulated in future sites of lung cancer metastasis [15]. These findings suggest that fibronectin plays a yet undefined role in the early development of tumors.

The aim of this study was to examine whether deletion of fibronectin in the bone marrow and in the circulation affects the development of breast and prostate cancer cells in the bone marrow niches and to identify the mechanisms underlying these effects. We found that circulating fibronectin enhances tumor growth by increasing vascular endothelial growth factor (VEGF) content, VEGF-mediated signaling, and blood vessel formation.

Materials and Methods

Mice

Mice possessing an Mx or albumin promoter driving cre-recombinase expression were crossed with mice carrying *loxP*-flanked (floxed) fibronectin [5] and foxn1 mutation [16]. The presence of homozygote foxn1 mutations results in immune deficiency. Mx was induced at 3 weeks with three injections of polyinosinic–polycytidylic acid (pIpC; 250 μg; Amersham, Freiburg, Germany) [5]. Enhanced green fluorescent protein (eGFP) reporter mice, in which cells expressing cre produce eGFP and, hence, fluoresce [17], were backcrossed to the above lines as noted in the text. Growth and homing experiments as well as most of the experiments reported in conditional knockout (cKO) animals used littermates as controls. Plasma fibronectin was determined by ELISA from tail-vein blood [18]. To determine bone marrow fibronectin, the bone marrow was flushed with 100 μl of protein lysis buffer/femur, and fibronectin was determined by ELISA corrected to protein content by BCA (Pierce, Bonn, Germany) [10,19,20]. To evaluate the cell types in which fibronectin is deleted due to the presence of cre, the bone marrow cells were flushed from mice carrying Mx-cre, which are homozygotes for floxed fibronectin and carry eGFP. eGFP is produced whenever a stop codon is removed due to the presence of cre. The cells that were exposed to cre recombinase therefore fluoresce green [17]. Cells were then stained with the antibodies described in the text and below under flow cytometry. For homing experiments, 10^5 cancer cells were injected intracardially, and 24 hours later, DNA was extracted and examined by quantitative polymerase chain reaction (qPCR) for human alu. Results are adjusted to murine bone marrow [14,21].

For intracardiac injection of cancer cells, mice were anesthetized (ketamine/xylazine), and 10^5 cancer cells per 100 μl of phosphate-buffered saline were injected into the left ventricle [22]. Tumor growth was evaluated weekly starting 3 weeks after injection by bioluminescence imaging (BLI). Total bioluminescence signal describes the total tumor burden per mouse [22].

Intratibial injection was performed as described [22]. Briefly, mice were anesthetized, and two holes were drilled in the left tibia. Bone marrow was flushed out from the upper hole, which was then sealed. Cancer cells (5×10^4 per 5 μl of phosphate-buffered saline) were injected in the lower hole using a Hamilton pipette (75RN;31/2″/3S), the hole sealed, and the skin sutured. Tumor growth was monitored starting day 7 and up to 40 days by BLI. Bromodeoxyuridine (BrdU; 100 mg/kg) was injected 1 hour before euthanasia. Tumors obtained at day 40 were used for histology, protein, and mRNA tests.

BLI was performed using IVIS-100 5 minutes after D-luciferin (150 mg/kg) (Synchem, Felsberg, Germany) injection. Lytic lesions were detected by radiography using a Faxitron. Lytic lesions on X-rays were analyzed using ImageJ (Wayne Rasband, NIH, Bethesda, MD).

For detection of injected fibronectin in tumors, labeled fibronectin (1 mg) was injected every 12 hours thrice intraperitoneally in mice that received intratibial cancer cell injections 18 days earlier. Mice were killed 6 hours after the last injection. Labeling was performed using Oyster-488 (Dianova, Hamburg, Germany) according to the manufacturer's protocol. Unlabeled fibronectin was removed using Sephadex columns (GE Healthcare, Freiburg, Germany). Labeled fibronectin was assessed in a sandwich ELISA confirming maintenance of binding and expected concentration. Masson-Goldner staining to confirm the presence of tumor was performed as described [10]. The experiment was repeated twice with similar results.

Staining Protocols and Immunohistochemistry

Cryosections of 3.7% neutral-buffered formalin-fixed tumors were stained with the following antibodies: rat anti–mouse CD31 (AbD Serotec, Düsseldorf, Germany), mouse anti–alpha-smooth muscle actin (α-SMA)-Cy3 (Sigma-Aldrich, Taufkirchen, Germany), sheep anti-fibronectin, sheep anti-BrdU (Biozol, Eching, Germany), rabbit anti-desmin, goat anti–sheep-Cy3 (Dianova), rabbit anti–von Willebrand factor (vWF; Axxora, Lörrach, Germany), rabbit anti–active caspase-3 (Abcam, Cambridge, United Kingdom), goat anti–rat-Cy2, or goat anti–rabbit-Alexa-555 (Molecular Probes, Invitrogen, Darmstadt, Germany). For chromogen staining, EnVision kit (Dako, Hamburg, Germany) was used. Sections were photographed using a Nikon-90i microscope and processed using ImageJ. Quantification was performed in at least three sections per mouse in at least three mice per group or more as noted in the figure legends. At least 0.9 mm^2 was examined per section.

Cell Isolation and Culture

MDA-MB-231B/luc$^+$ or PC-3M-Pro4/luc$^+$ was cultured in Dulbecco's modified Eagle's medium (DMEM)/10% fetal calf serum (FCS) with 800 and 500 μg/ml geneticin, respectively [22]. Cells were counted using an automated cell counter (CASY-TT; Innovatis, Mannheim, Germany). For some experiments, fibronectin-depleted FCS was

obtained by running FCS on gelatin-Sepharose columns three to five times and dialysing against FCS [18]. Successful depletion was confirmed by ELISA, and final concentration of fibronectin was 8 to 11 ng/ml.

Isolation of tumor endothelial cells was performed as described with modifications [23,24]. Briefly, tumors were minced, digested [1 mg/ml collagenase-A (Serva, Heidelberg, Germany) + 0.05% DNAse1 (Roche, Mannheim, Germany) at 37°C for 45 minutes with shaking], filtered, and centrifuged. Pellets were washed and resuspended in DMEM/10% FCS. Dynabeads (30 µl; Invitrogen) were precoated with 20 µg of rat anti-CD31 antibody [MEC 7.46] (Abcam). Cells were added for 1 hour at 4°C, beads were washed, and cells were released with 0.05% trypsin/EDTA (Gibco, Invitrogen) and cultured in DMEM/20% FCS, 2 mM L-glutamine, 2 mM sodium pyruvate, 20 mM Hepes, 1% nonessential amino acids, 100 µg/ml streptomycin, 100 UI/ml penicillin, 12 U/ml heparin (fresh), and 100 µg/ml EC growth supplement (Sigma). Passages 3 to 5 were used. To determine fibronectin production, cells were cultured for 72 hours in the presence of 20% fibronectin-depleted FCS.

Pericytes were isolated from the bone marrow using Dynabeads (Invitrogen) coated with CD45 (clone 30-F11; BioLegend, Fell, Germany) followed by Dynabeads coated with rat anti–mouse-angiopoietin-1 (Abcam). Angiopoietin-1–coated beads were treated with RNA lysis buffer or cultured for 24 hours in the presence of 10% fibronectin-depleted FCS. Pericytes stained for angiopoietin-1 were also sorted using FACSVantage and cultured or examined by flow cytometry for α-SMA staining.

Proliferation was performed as follows: 27,000 cells per 200 µl of DMEM either without FCS (cancer) or with 20% fibronectin-depleted FCS (endothelial cells) were seeded, cultured for 36 (cancer) or 48 hours (endothelial cells), and counted as above. For endothelial cells, fibronectin was added at 200 µg/ml and recombinant human VEGF-165 (*Spodoptera frigiperda*; R&D Systems, Abingdon, United Kingdom) at 6 ng/ml. Signaling molecules were examined in cells seeded overnight and activated with fibronectin, VEGF, or both without FCS for 15 minutes, and the reaction was stopped on ice followed by washing twice. BCA was used to quantify protein content (Pierce), and 100 µg was loaded onto each lane in 10% gels.

Fibronectin assembly was inhibited by daily adding 500 nM FUD [25] and compared to scrambled peptide, 200 µg/ml fibronectin, or no addition. In another experiment, cells were treated either with 200 µg/ml fibronectin, 6 ng/ml VEGF, both fibronectin and VEGF, or left untreated. Substances were added directly after plating 10^6 cells in 2 ml/well of a six-well-plate (total FN, 400 µg and total VEGF, 12 ng). In both experiments, cells were left in culture for 72 hours, then treated with 1% deoxycholate as described [8]. The insoluble fraction (DOC insoluble) represents matrix. Fibronectin and human VEGF ELISA results were corrected to total protein.

Flow Cytometry

Bone marrow was flushed from femora as described above, and cells stained with the following antibodies: rat anti–plasma-lemma-vesicle-associated protein–AF-647 (MECA-32; AbD Serotec), rat anti–CD31-PE (clone MEC13.3; BioLegend), rabbit anti-desmin, mouse anti–α-SMA-Cy3 (Sigma-Aldrich), rat anti–mouse-angiopoietin-1 (Abcam), goat anti–rabbit-Cy3 (Dianova), and rat anti–CD45-Pacific Blue or APC-Cy7 (clone 30-F11; BioLegend). Flow cytometry was performed using LSR-2 (BD Biosciences, Heidelberg, Germany). Examination of eGFP expression in pericytes was performed on stroma obtained from the bone marrow after depletion using CD45-coated Dynabeads.

For Annexin V/propidium iodide (AV/PI) staining, tumors were minced and digested, and 10^6 cells were resuspended in 50 µl of AV/PI binding buffer [10 mM Hepes (pH 7.4), 140 mM NaCl, and 2.5 mM $CaCl_2$]. AV (12.5 µg/µl) and PI (1 µg/ml) were added (BioLegend) for 30 minutes at room temperature in the dark, and samples were measured within 20 minutes.

DNA Analysis

Genomic DNA was isolated from femora using DNeasy Blood and Tissue Kit (Qiagen, Hilden, Germany). Real-time qPCR was performed using LightCycler 2.0 (Roche) using the primers and probes for alu as described [21]. Results were normalized to murine β-actin. An external standard curve using known numbers of human and mouse cells was created for both alu and β-actin. We were able to detect 0.2 cancer cell/10^6 mouse cells.

RNA Analysis

RNA was isolated using RNeasy (Qiagen) and reversed transcribed using iScript-Select (Bio-Rad, Munich, Germany). qPCR results were normalized to murine β-actin or human HPRT. The probes used were given as follows: murine fibronectin #66; human fibronectin #76; human HPRT #22; murine β-actin #64; RGS5 #31 [26]; VEGF-A, both human and murine #64 with different primers; murine VEGF receptor 2 (VEGFR-2) #62. The primers used were those suggested by Roche universal probe library except for human fibronectin: 5′actgagactccgagtcagcc, 3′ttccaacggcctacagaatt.

Protein Analysis

For Western blot analysis, the following antibodies were used: anti–fibronectin-HRP (Dako), β-tubulin (Sigma-Aldrich), Bcl-2, BAX (BD Pharmingen, Heidelberg, Germany), extracellular signal-regulated kinase (ERK), pERK, AKT, pAKT, stress-activated protein kinase/Jun amino-terminal kinase (SAPK/JNK) kinase, pSAPK/JNK kinase, VEGFR-2, pVEGFR-2 (Cell Signaling Technology, Frankfurt, Germany), focal adhesion kinase (FAK; Millipore, Schwalbach, Germany), and pFAK (Biosource, Invitrogen). All antibodies were diluted 1:1000. Samples were loaded after adjusting to protein content measured by BCA (Pierce).

Fibronectin was quantified in mouse plasma, cell lysates, and conditioned media by ELISA as reported [18,19] and corrected to protein content measured by BCA (Pierce) when appropriate. Briefly, plates were coated with the primary antibody (0.12 µg/ml, F3648; Sigma). For mouse plasma, bone marrow lysates, conditioned media of endothelial cells, and tumor samples, the standard used was murine plasma fibronectin (#IMFBN; Dunn, Asbach, Germany). For tumor lysates, the standard used was human plasma fibronectin isolated as described [10]. The secondary anti–fibronectin-HRP antibody (P0246; Dako) was used.

VEGF was quantified in tumor tissue samples lysed in protein lysis buffer and applied in mouse and human VEGF ELISAs (dilution of 1:5 and 1:8, respectively) as well as in cell culture material (dilution of 1:5 and 1:2 for medium and DOC soluble and insoluble fractions according to the manufacturer's recommendations, respectively; R&D Systems).

Patients

Tumor tissue samples from three tissue microarrays were stained. Samples were evaluated for intensity of staining and scored on a scale of 0 to 2 by a person blinded to the follow-up data. The breast cancer tissue microarray included 100 primary tumor samples of untreated patients diagnosed and operated upon in the years 2003 to 2007 with a follow-up until January 2012 (median follow-up of 88 months). Patient survival data of the first untreated prostate cancer array were available for at least 5 years after diagnosis. The second prostate array included primary tumors of 116 untreated patients operated in 2002 to 2004 with follow-up until 2011 (median follow-up of 73 months).

Statistical Analyses

Analyses were performed using SPSS (V20). Analysis of variance and repeated measures analysis of variance tests were used as appropriate. If global probability values were smaller than 5%, subsequent comparisons between selected group pairs were then performed using Student's *t*, Mann-Whitney, or Wilcoxon paired tests as appropriate. Pearson correlations were estimated to evaluate the relationship between two variables. The 5-year survival rates from patients in the first prostate array were explored using a Jonckheere-Terpstra exact test (SAS), which takes into account the ordering of staining intensities. The other two patient collectives were investigated by relying on Kaplan-Meier survival curves and Cox regression. Results are expressed as means ± SEM.

Results

Deletion of Fibronectin Using the Albumin or Mx Promoter Attached to Cre

Our aim was to examine the role of fibronectin in the formation of bone metastases. We used an MDA-MB-231B/luc+ human cancer cell line that has been selected for its ability to home to the bone marrow and reliably establish bone metastases [22]. This cancer line needs to be applied into mice that are immune deficient. We therefore used mice homozygote for the *foxn1*^{nu} mutation making them nude and resulting in absence of functional T-cells and inability to reject the human cancer cells [16].

Since fibronectin knockout mice die *in utero*, we used two cKO models in the immune-deficient mice: The albumin promoter attached to cre recombinase is spontaneously active and results in a gradual deletion of fibronectin in the hepatocytes and, hence, a slow loss of circulating fibronectin that is completed by 8 weeks of age in mice that are homozygote for the floxed fibronectin gene (Alb-cKO). The second promoter, the Mx promoter, attached to cre recombinase [5] can be activated in 3-week-old homozygote fibronectin-floxed mice by injecting polyinosinic–polycytidylic acid. This results in deletion of circulating fibronectin already by 4 weeks of age, because the Mx promoter is also active in hepatocytes (Figure 1*A*). Unlike the Alb-cKO model that is specific for circulating fibronectin, the Mx-cKO model results in deletion of fibronectin in the bone marrow (Figures 1*B* and W1*A*). To determine which cell types in the bone marrow undergo deletion in the Mx model, we used eGFP reporter mice that were homozygotes for the fibronectin-floxed gene [17]. Cells in which cre recombinase is activated should both express eGFP and show deletion of fibronectin, and hence, the number of eGFP-expressing cells will be higher in Mx-cKO mice. In Mx-cKO, eGFP was expressed in CD45+ cells, endothelial cells [27], sinusoidal cells [28], and pericytes (Figure 1*C*) [29,30]. Using both cKO models, we should be able to define the role of circulating fibronectin and find out whether bone marrow fibronectin affects cancer development.

Deletion of Fibronectin in the Circulation Affected Tumor Growth

We sought to examine the role of fibronectin in homing of cancer cells to the bone marrow and early growth of bone metastases. The above-mentioned MDA-MB-231 cell line expresses luciferase (luc+), and therefore, BLI could be used to monitor tumor development longitudinally (Figure W1*B*) [22].

Intracardiac injection of cancer cells is performed in 4-week-old mice, when bone lesions reliably form in all mice. At 4 weeks, fibronectin in the circulation was decreased by 95% in Mx-cKO and 40% in Alb-cKO mice (Figure 1*A*) for the reasons discussed above. Fibronectin in the bone marrow is only affected in Mx-cKO, however (Figures 1*B* and W1*A*). Thus, if bone marrow fibronectin does not affect tumor growth, the intracardiac model allows for a comparison between the effect of a small and a large decrease in circulating fibronectin levels. Intracardiac cancer cell injection in Mx-cKO and Alb-cKO mice did not affect the number of tumor lesions compared to littermate controls (CT; Figure W1*C*) nor the number of cancer cells that homed to bone marrow [21] (Figure W1*D*). There were two differences nevertheless. Only in Mx-cKO was tumor burden per mouse decreased (Figure 1*D*), and median survival was increased from 6.6 weeks in CT to 8.6 weeks in Mx-cKO ($P < .05$; Figure 1*E*). These data suggest that prolongation of survival and decreased tumor burden in Mx-cKO mice is not due to decreased homing to the bone marrow but to decreased growth. Furthermore, the normal growth in Alb-cKO suggests that either a decrease in circulating fibronectin by 40% does not affect tumor growth or that bone marrow fibronectin is critical for tumor growth.

To differentiate between these two possibilities, a role of circulating fibronectin or bone marrow fibronectin, we looked for a model that can be used in 8-week-old mice when both Alb-cKO and Mx-cKO mice show similar deletion in circulating fibronectin (Figure 1*A*). Intratibial injection of cancer cells is usually performed at this age [22]. Induction of a single bone lesion in the tibia offers an additional advantage of providing comparable tissue samples for further studies [22]. Using this model, tumor growth in Mx-cKO and Alb-cKO mice was similarly decreased by 50% (Figure 1*F*). This was confirmed by a decrease in cancer-induced osteolysis at the site of tumor growth (Figure W1*E*). Since at the age of 8 weeks Alb-cKO and Mx-cKO only differ in the absence of fibronectin in the bone marrow of Mx-cKO, these data suggest that circulating fibronectin and not bone marrow fibronectin affected tumor growth.

To determine whether the effects of circulating fibronectin can be reproduced in other cancer types, we used the prostate cancer cell line PC3Mpro4/luc+. Intratibial injection in CT, Mx-cKO, and Alb-cKO mice showed similar effects to those described (Figure W2). Thus, the conclusion that circulating fibronectin affects tumor growth is not limited to MDA-MB-231.

Circulating Fibronectin Infiltrates Tumor Tissue and Modulates Its Own Production in Tumor

Since circulating fibronectin affected tumor growth, we asked whether this effect might be due to infiltration of circulating fibronectin into tumor tissue. Two results supported this conclusion.

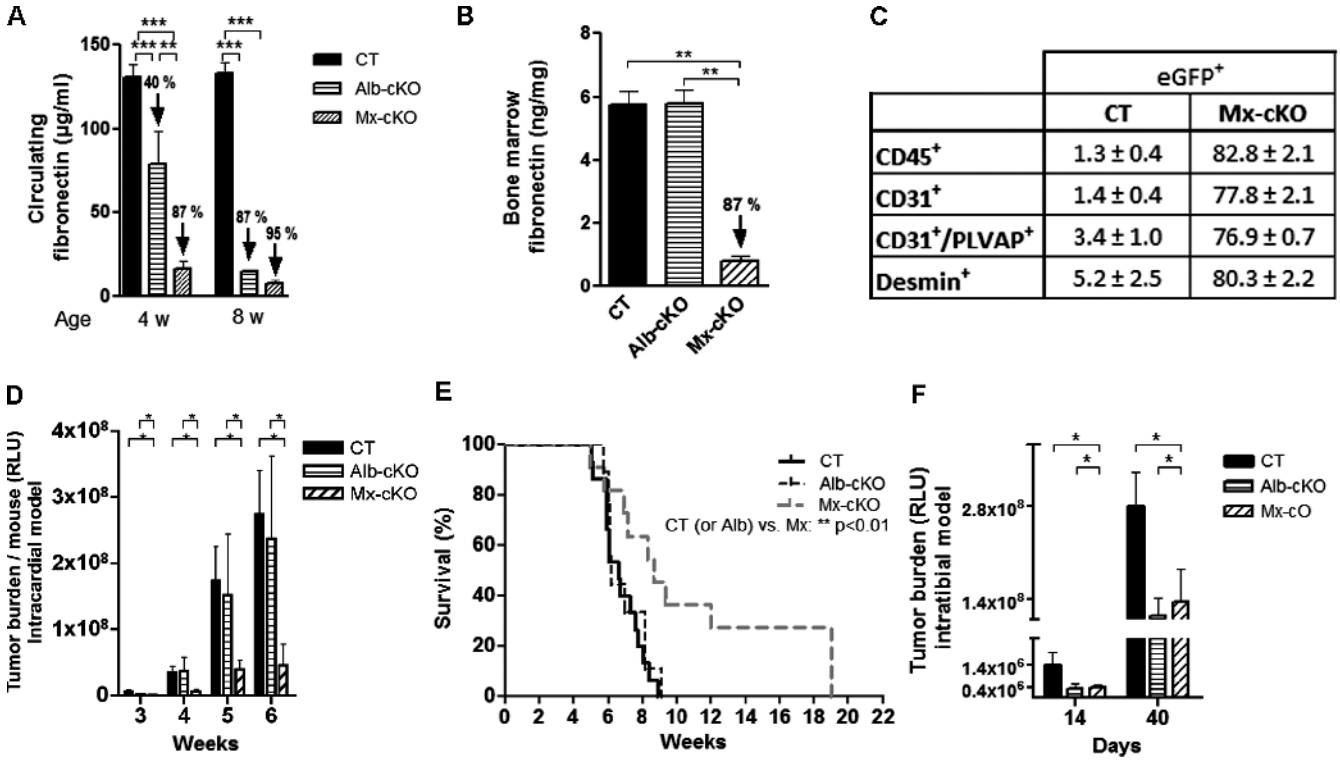

Figure 1. Deletion of fibronectin in Mx-cKO and Alb-cKO mice affects tumor development. (A) Circulating fibronectin in Alb-cKO mice is decreased by 40% at 4 weeks and 87% at 8 weeks of age, while levels in Mx-cKO were decreased by 87% and 95% compared to controls (CT) as determined by ELISA (N = 9-11/time point per group). (B) Deletion of fibronectin in the bone marrow in Mx-cKO is successful and stable for at least 2 weeks after the last pIpC injection, while deletion of circulating fibronectin did not affect fibronectin amount in the bone marrow of Alb-cKO mice. Bone marrow was flushed with 100 µl of protein lysis buffer/femur. Fibronectin was measured by ELISA and corrected to protein content measured by BCA (N = 3/group). (C) Use of the Mx promoter leads to deletion of fibronectin in leukocytes (CD45+), endothelial cells (CD31+), sinusoidal cells (CD31+/PLVAP+), and pericytes (desmin+). Bone marrow was flushed from mice that express eGFP in cells in which the Mx promoter was activated and, hence, are green, stained, and examined by flow cytometry. (D) The total bioluminescence signal (tumor burden/mouse) was similar between CT and Alb-cKO but was smaller in Mx-cKO after intracardiac injection (N = 11-12/group). (E) Median survival was increased by 2 weeks in Mx-cKO. (F) Intratibial injection is associated with a decrease in bioluminescence signal in both Alb- and Mx-cKO starting at day 14 post-injection until the end of the experiment at day 40 (N = 9-11/group). The values on the y-axis represent mean bioluminescence signal of the bars shown. *P < .05, **P < .01, ***P < .0001.

First, injected prelabeled plasma fibronectin could be detected in tumor tissue (Figure 2*A*), and second, the decrease in circulating fibronectin found in Mx-cKO and Alb-cKO was associated with a decrease in fibronectin content in both Mx- and Alb-cKO tumors compared to CT as determined by staining intensity and protein amounts measured by ELISA (Figure 2, *B* and *C*). The amount of fibronectin measured by ELISA in tumor tissue in Mx- and Alb-cKO was about 1/10th that in CT (Figure 2*C*).

It has been suggested that fibronectin increases its own production [31]. We therefore examined whether the decrease in circulating fibronectin and, hence, fibronectin infiltration affected the amount of fibronectin produced locally in tumor tissue. To do, this we designed human- and mouse-specific primers for fibronectin. Species specificity in qPCR was confirmed. Both local cancer cell (human) and stromal (murine) fibronectin production were diminished in Alb-cKO and Mx-cKO (Figure 2*D*). This suggests that circulating fibronectin infiltrating the tissue enhances the amount of local fibronectin produced. Thus, both diminished circulating fibronectin and suppressed local fibronectin production contribute to a decrease in fibronectin content in tumors.

Establishing the Reasons for Decreased Growth in the cKO Mice

Fibronectin has been implicated in blood vessel formation [32]. Furthermore, it directly stimulates proliferation and inhibits apoptosis [33]. Thus, the decrease in fibronectin content could, through these mechanisms, result in decreased tumor growth. We therefore evaluated these three possibilities.

Angiogenesis in vivo. We first evaluated the effect of circulating fibronectin on blood vessel formation. Because we had expected a more pronounced effect on growth in Mx-cKO mice, we first determined whether Mx was indeed able to delete fibronectin in vascular cells. We therefore isolated tumor endothelial cells and marrow pericytes from Mx-cKO mice using CD31 and angiopoietin-1 antibodies, respectively. Isolated endothelial cells stained with vWF (98%) and pericytes with α-SMA (97%; Figure W3, *A* and *B*). Successful fibronectin deletion was confirmed in both cell types originating from Mx-cKO mice compared to CT by measuring fibronectin protein in conditioned media using ELISA (Figure 3, *A* and *B*). Evaluation of the vascular supply by staining for CD31 in tumor sections revealed diminished vascularization per unit area in tumors from both

cKOs using both breast and prostate cancer cell lines (Figures 3, *C* and *D*, and W4). There was no difference however between Mx- and Alb-cKO tumors in vessel density despite the successful deletion of fibronectin in endothelial cells and pericytes in Mx-cKO mice. Thus, the decrease in blood vessel numbers was not affected by fibronectin production in vascular cells.

Because pericyte recruitment and, hence, blood vessel maturation are affected by extracellular matrix proteins including fibronectin [30,34], tumor sections were stained with both α-SMA to detect pericytes and CD31 to detect endothelial cells. The percentage of blood vessels (identified by CD31 staining) that, at the same time, showed α-SMA–stained cells was smaller in cKOs, suggesting that

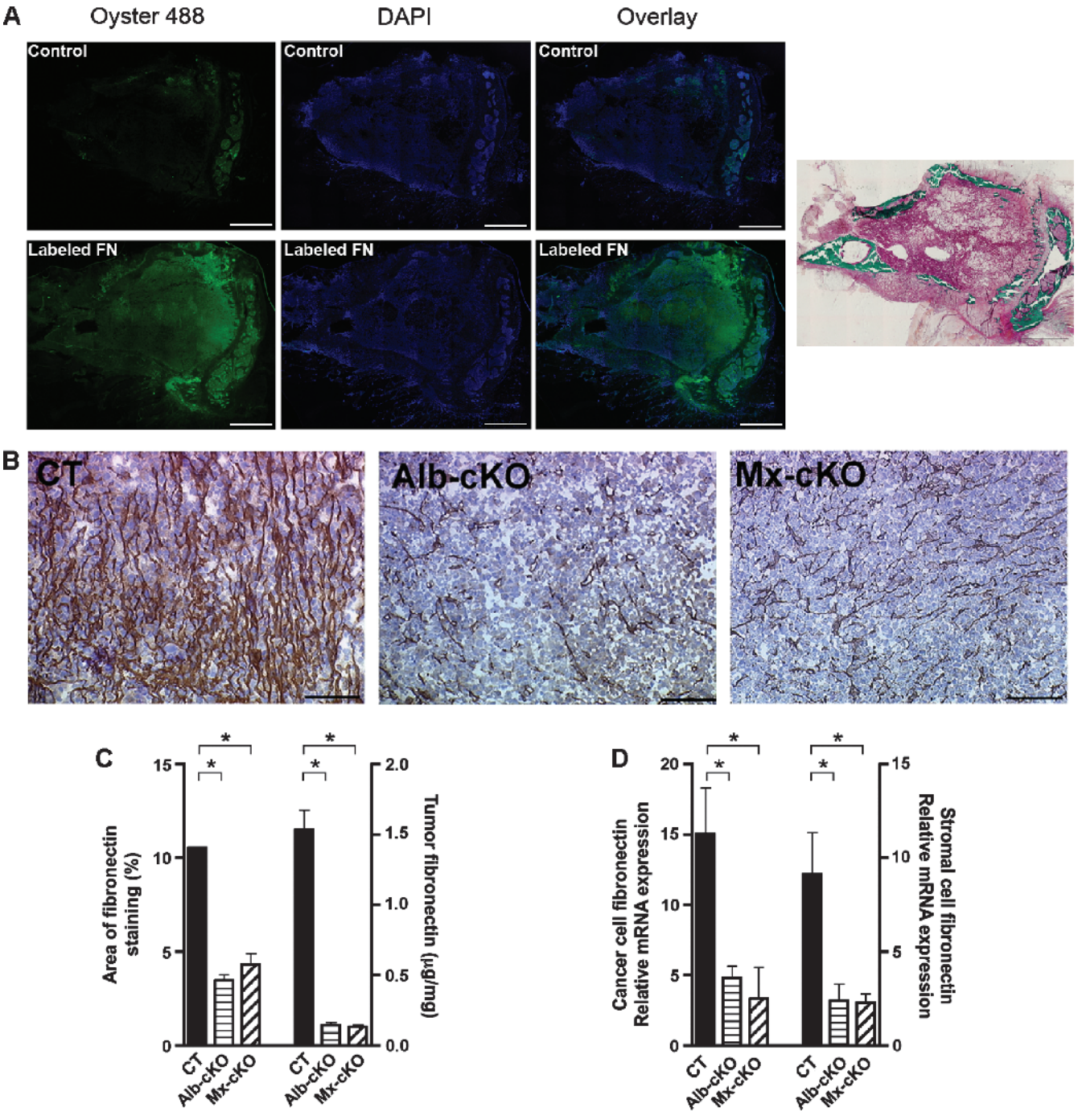

Figure 2. The role of circulating fibronectin. (A) Labeled fibronectin can be detected within the tumor after injection. Masson-Goldner stain confirms the presence of cancer. Bars represent 500 μm. (B) Fibronectin staining was diminished in Alb- and Mx-cKO tumors. Bars represent 100 μm. (C) Quantifying the area of staining showed a decrease by more than 60% in Alb- and Mx-cKO tumors compared to controls (N = 3-4 mice/group). Similarly, quantifying the amount of fibronectin in tumors by ELISA reveals that CT tumors had more than 10-fold higher fibronectin content compared to Alb-cKO and Mx-cKO tumors. Fibronectin was examined by ELISA and values adjusted to protein (N = 3-6/group). (D) Both cancer cell fibronectin mRNA expression corrected to human HPRT and stromal fibronectin mRNA expression corrected to murine α-actin are decreased in Alb- and Mx-cKO (N = 4/group). *P < .05, **P < .001.

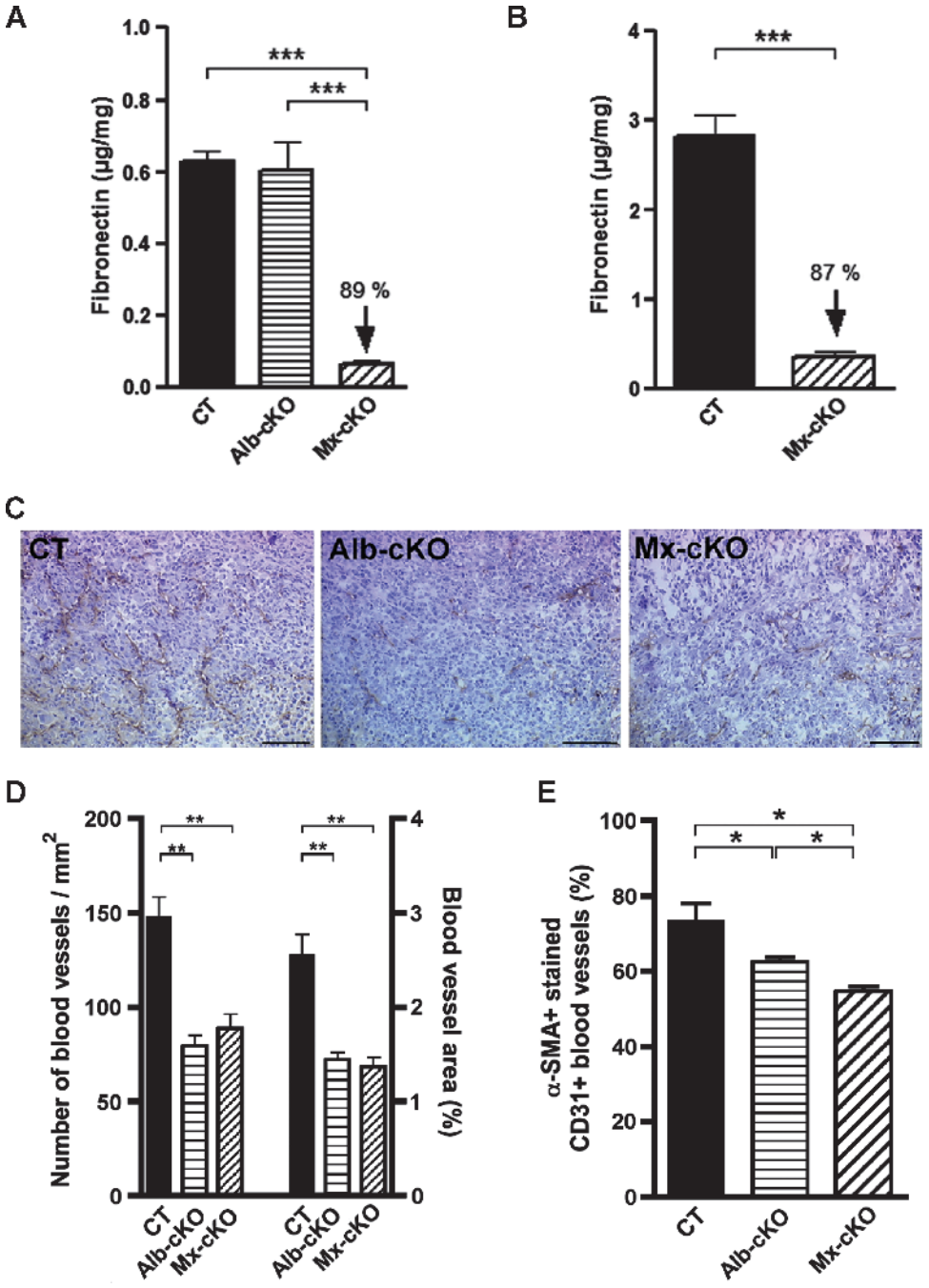

Figure 3. Effects of fibronectin on angiogenesis. (A) Conditioned media from endothelial cells originating from Mx-cKO tumors do not produce fibronectin compared to endothelial cells originating from Alb-cKO or CT tumors (N = 3-5 replicates/group). (B) Fibronectin production in conditioned media is decreased in pericytes from Mx-cKO mice. Isolated cells were cultured for 24 hours. (C) Sections from CT, Alb-, and Mx-cKO intratibial tumors show a difference in the number of CD31-stained blood vessels. Bars represent 100 μm. (D) The number of CD31-stained blood vessels as well as the area covered by these vessels was decreased in Alb- and Mx-cKO tumors at 40 days post-injection (N = 6 tumors/group, six sections/tumor). (E) The percentage of blood vessels co-stained for CD31 and α-SMA was evaluated. The decrease in the percentage of α-SMA+ blood vessels was more pronounced in Mx- than in Alb-cKO tumors. For the purpose of this graph, the number of CT, Alb-cKO, and Mx-cKO CD31+ vessels was set at 100% (N = 3, 3, 6 mice, four sections/mouse). *P < .05, **P < .01, ***P < .0001.

the absence of fibronectin leads to decreased vessel maturation (Figures 3*E* and W5, *A*–*C*). These findings were confirmed by staining with desmin, another pericyte marker together with CD31 (Figure W5, *D* and *E*). Nevertheless, the percentage of vessels covered with pericytes was higher in Alb- compared to Mx-cKO (Figures 3*E* and W5*E*). Lastly, mRNA for the pericyte marker RGS5 in tumor tissue [26] was also diminished in cKO tumors (Figure W5*F*).

On the basis of these findings, we conclude that circulating fibronectin plays a key role in tumor growth by supporting blood vessel formation. Blood vessel maturation, however, is controlled by both vascular fibronectin and circulating fibronectin.

Effects on VEGF and VEGF-mediated signaling. Fibronectin has multiple binding sites for VEGF [35] and fibronectin matrix functions as a reservoir for VEGF [9]. We therefore examined whether VEGF is affected in tumor samples. To differentiate between VEGF originating from cancer and stromal cells, two species-specific ELISA kits against human (hence cancer cell) and murine (hence, stromal cells) VEGF were used. Testing of tumor tissue *ex vivo* revealed a significant decrease in cancer cell VEGF protein corrected to total protein but not stromal VEGF as measured in the respective ELISAs (Figures 4*A* and W6*A*). The decrease in cancer cell VEGF protein was not associated with a change in cancer cell VEGF mRNA expression (Figure W6*B*), suggesting that storage of VEGF was diminished in cKO tumors. To test this *in vitro*, cancer cells were cultured in the presence of fibronectin-depleted FCS without additives, in the presence of a peptide that prevents fibronectin deposition (called FUD) [25], a scrambled peptide, or added fibronectin to the medium (200 μg/ml). Matrix fibronectin was decreased in the presence of FUD and increased in the presence of added fibronectin. Concordant changes in matrix VEGF could be detected (Figure 4*B*, *right axis*). Furthermore, the addition of fibronectin to the medium resulted in an increase in the matrix of retrieved endogenous VEGF (Figure 4*C*, *left two bars*) as well as exogenously added VEGF (*third* and *fourth bars*). VEGF in media or cell lysates did not differ however (data not shown). These data suggest that indeed the presence of fibronectin in the matrix contributes to retention of VEGF in the matrix and that in cKO tumors the decrease in fibronectin content contributes to loss of VEGF from the matrix.

We next asked whether the decrease in VEGF affected signaling. Because the proangiogenic effects of VEGF are mainly mediated through VEGFR-2, we first established murine- and human-specific qPCR primers for VEGFR-2. Murine VEGFR-2 mRNA expression was diminished in tumor samples from cKO mice, while human VEGFR-2 was not changed (Figures 4*D* and W6*C*), suggesting that the decrease in VEGF in tumors was associated with a decrease in the expression of its receptor on murine stromal cells. Furthermore, the amount of phosphorylated VEGFR-2 was diminished in cKO tumors, suggesting that signaling through this receptor was also diminished (Figure 4*E*).

These data support the conclusion that the amount of stored VEGF as well as VEGF-mediated signaling is diminished *in vivo* in Mx- and Alb-cKO tumors. Thus, the amount of fibronectin in tumors seems to control signaling by VEGF.

Fibronectin cooperates with growth factors to induce intracellular signals [36]. We therefore asked whether the decrease in stored VEGF solely was responsible for decreased blood vessel formation or whether the decrease in fibronectin contributed to the decrease in VEGF-mediated signaling in our model. To begin to address this issue, we used proliferation as a proxy measure for collaboration of both fibronectin and VEGF. Proliferation of tumor endothelial cells *in vitro* was significantly increased by either adding fibronectin or VEGF to endothelial cells isolated from CT tumors (Figure 4*F*). Proliferation of Mx-cKO cells was increased by the addition of fibronectin but was not changed by VEGF alone, presumably because of the absence of endogenous fibronectin shown above (Figure W6*D*). The combination of fibronectin and VEGF resulted in the best response in endothelial cells, however. Thus, fibronectin and VEGF seem to exert synergistic effects on proliferation. In support of these findings, both phospho-ERK and phospho-AKT increased in the presence of both fibronectin and VEGF and, in the case of phospho-AKT, more so than when either one was added alone, while neither phospho-FAK nor phospho-JNK showed significant changes (Figures 4, *G–I*, and W6, *E* and *F*). This is in line with an additive effect of fibronectin and VEGF on cells.

Thus, circulating fibronectin infiltrates tumor tissue, increases local fibronectin production and VEGF retention, and together with VEGF potentiates intracellular signals and, hence, increases blood vessel formation. It thus seems that in this context fibronectin is more relevant for tumor growth than VEGF.

Effects on proliferation and apoptosis. Fibronectin can directly affect proliferation [33]. We therefore evaluated BrdU incorporation in tumors *in vivo* by staining and found that proliferation was indeed diminished in cKO (Figure 5, *A* and *B*). We confirmed a direct effect of fibronectin on proliferation by showing a dose response in cancer cells *in vitro* to fibronectin, whereby proliferation in response to 500 μg/ml fibronectin was equivalent to 10% fibronectin-depleted FCS (Figure 5*C*) establishing a proliferative role for fibronectin on our tumor cells that is equivalent to the growth factors found in FCS.

Apoptosis in tumors was increased in cKO mice as measured by terminal deoxynucleotidyl transferase dUTP nick end labeling (TUNEL) staining in sections (Figure 5, *D* and *E*). This was confirmed in cell suspensions from tumors treated with collagenase and stained with AV and PI (Figure W7, *A* and *B*). This increase was not mediated by an effect on cleaved caspase-3 evidenced by lack of a difference in staining between CT and cKOs (Figure W7, *C* and *D*). It has been reported that an increase in BAX can mediate mitochondrial damage and cell death without caspase-3 involvement [37]. In line with this but unlike published reports on the effects of fibronectin in apoptosis [38], the expression of the antiapoptotic protein Bcl-2 was the same, but the proapoptotic protein BAX was higher in cKO (Figure 5*F*). This suggests that the increase in cell death is mediated by an increase in BAX.

Taken together, these data suggest that diminished fibronectin in tumor results in suppressed tumor growth due to decreased angiogenesis and proliferation and increased apoptosis.

Relevance for Human Cancer

Since fibronectin amount affects VEGF content, blood vessel formation, and growth, we asked whether in our murine model increased tumor fibronectin correlates with cancer growth. This was the case, whereby increased tumor fibronectin resulted in an increase in blood vessel formation and increased tumor burden (Figures 6, *A* and *B*, and W8).

To determine whether such an association could be reproduced in breast cancer patients, we examined an array of breast cancer biopsies of patients with a median follow-up of 88 months. Eighty-one samples could be evaluated for fibronectin staining. Fifty-four biopsies showed no staining, 18 weak staining, and 9 strong staining (Figure 6*C* and Table 1). Kaplan-Meier survival curves were not different between patients with tumors either without or with weak staining. Patients with tumors with strong staining intensity showed poorer survival (Figure 6*E*). Only fibronectin staining intensity and estrogen receptor status (ER) associated with cancer-specific survival (Table 1), whereby 8 of 9 tumors (89%) with strong staining intensity were ER negative compared to 34 of 72 tumors with no or weak fibronectin staining (47%; Figure 6*D*), and in the group in which ER was negative, strong fibronectin staining intensity correlated with decreased survival ($P < .05$). There was no correlation between fibronectin staining intensity and tumor size (T), nodal state (N), progesterone receptor (PR) status,

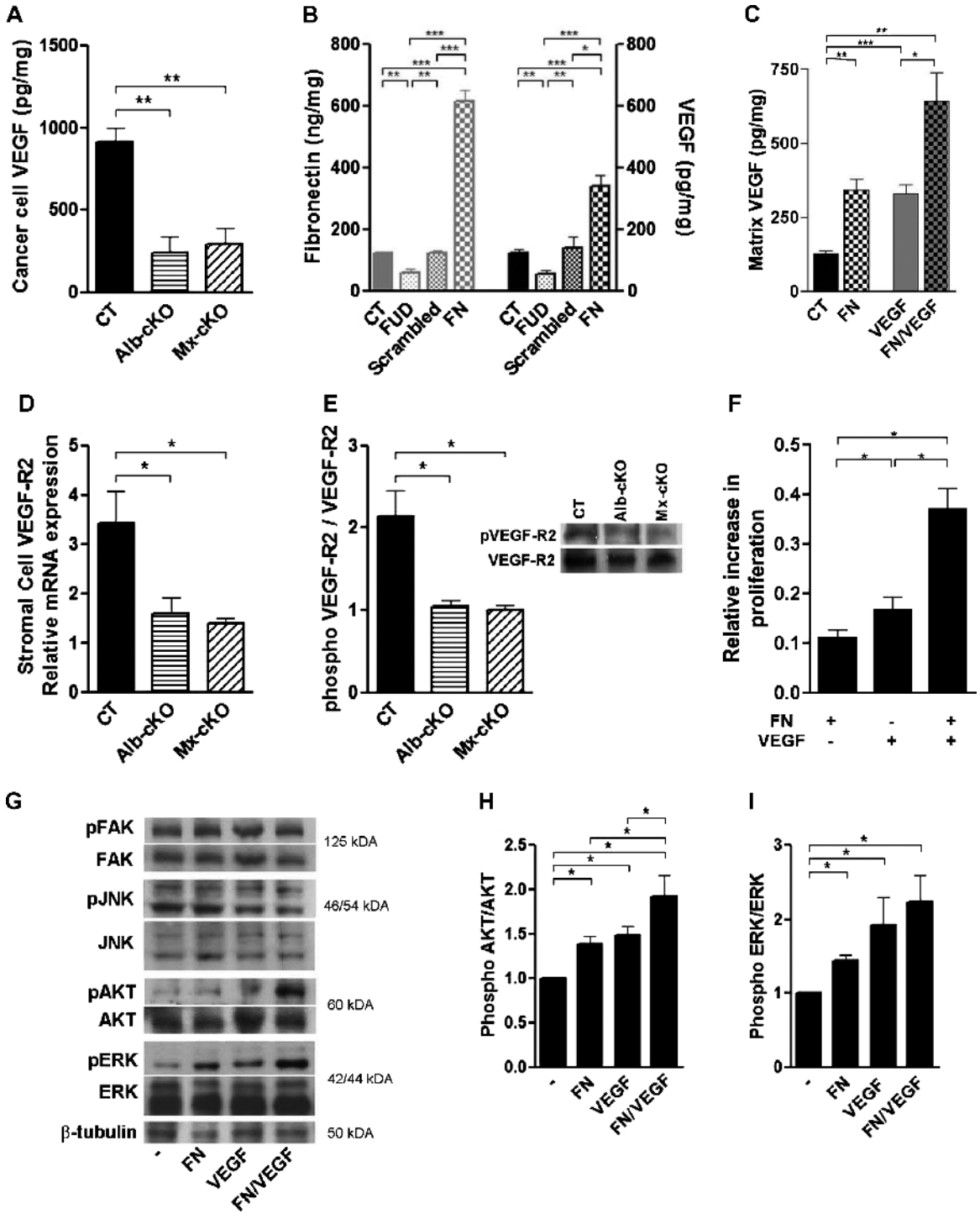

Figure 4. Mechanistic insights on the reason for decreased angiogenesis. (A) Cancer cell VEGF (by human-specific ELISA) was significantly diminished in tumors originating from cKO mice ($N = 4$-6/group). (B) A change in matrix fibronectin is associated with a concordant change in VEGF content in the matrix. Cancer cells were cultured in the presence of a peptide (FUD) that inhibits fibronectin deposition or in the presence of 200 μg/ml fibronectin (FN). Matrix was isolated on the basis of deoxycholate (DOC) insolubility, tested for fibronectin and VEGF by ELISA, and adjusted to total protein ($N = 4$-6/group). (C) Fibronectin retains both endogenous (CT *vs* FN) and exogenous VEGF (VEGF *vs* FN/VEGF) in the matrix. MDA cells were cultured for 72 hours in six-well plates without additives, in the presence of 400 μg of fibronectin, 12 ng of VEGF, or both. Matrix VEGF was quantified and corrected to protein in the DOC insoluble fraction as in B ($N = 3$-4/group). (D) Murine VEGFR-2 mRNA expression was diminished in cKO tumors, but human (Figure W6*C*) was not ($N = 4$/group). (E) The amount of phosphorylated VEGFR-2 was also diminished in cKO tumors in densitometry measurements. An example of a Western blot is shown on the right ($N = 4$/group). (F) Cell proliferation was significantly increased when endothelial cells were treated with either fibronectin or VEGF compared to untreated cells. The addition of both simultaneously resulted in a more pronounced increase in proliferation ($N = 3$ experiments with three to five replicates/condition per experiment). (G) Both phospho-ERK and phospho-AKT increased 15 minutes after the addition of both fibronectin and VEGF, while phospho-FAK and phospho-JNK did not. (H and I) Densitometries of phospho-AKT and phospho-ERK corrected to total AKT and ERK, respectively. $^*P < .05$, $^{**}P < .01$, $^{***}P < .0001$.

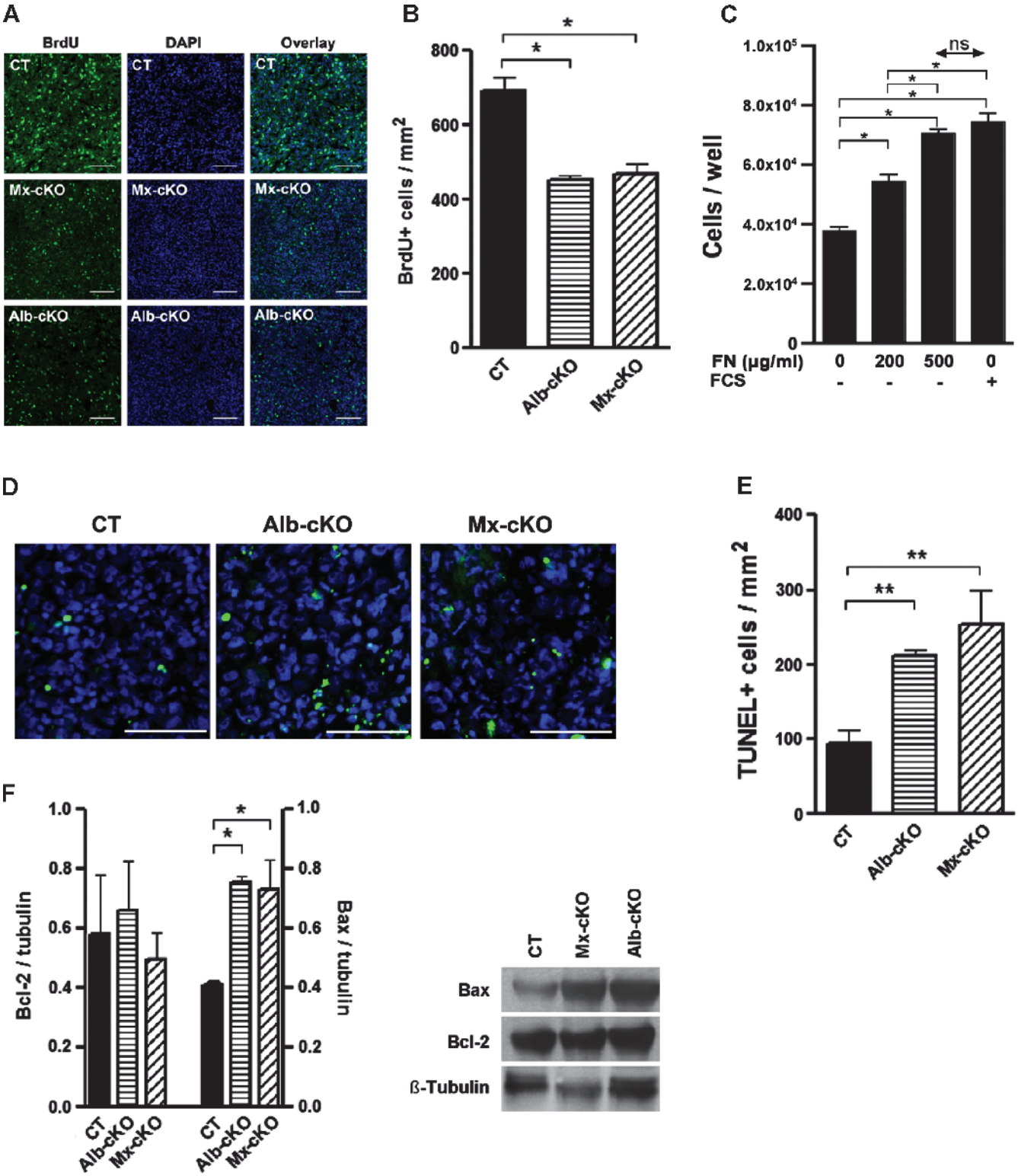

Figure 5. Effects of fibronectin content on proliferation and apoptosis. (A) The number of proliferating cells stained for BrdU in cKO tumors is diminished. Bars represent 100 μm. (B) Quantitative analysis of BrdU+ cells in tumors (N = 6 CT, 5 Alb-, and 5 Mx-cKO tumors). (C) Proliferation of tumor cells is improved by the addition of fibronectin. Fibronectin (500 μg/ml) and 10% fibronectin-depleted FCS increase proliferation to a similar extent. (D) TUNEL staining in tumor tissue from CT, Alb-, and Mx-cKO mice. Bars represent 200 μm. (E) The number of TUNEL-stained cells is increased in cKO tumors (N = 3-4/group). (F) Western blot analysis for Bcl-2 and BAX shows an increase in BAX in the absence of circulating fibronectin. A graph of densitometry of values adjusted to β-tubulin is shown on the left. On the right, an example is presented (N = 3/group).

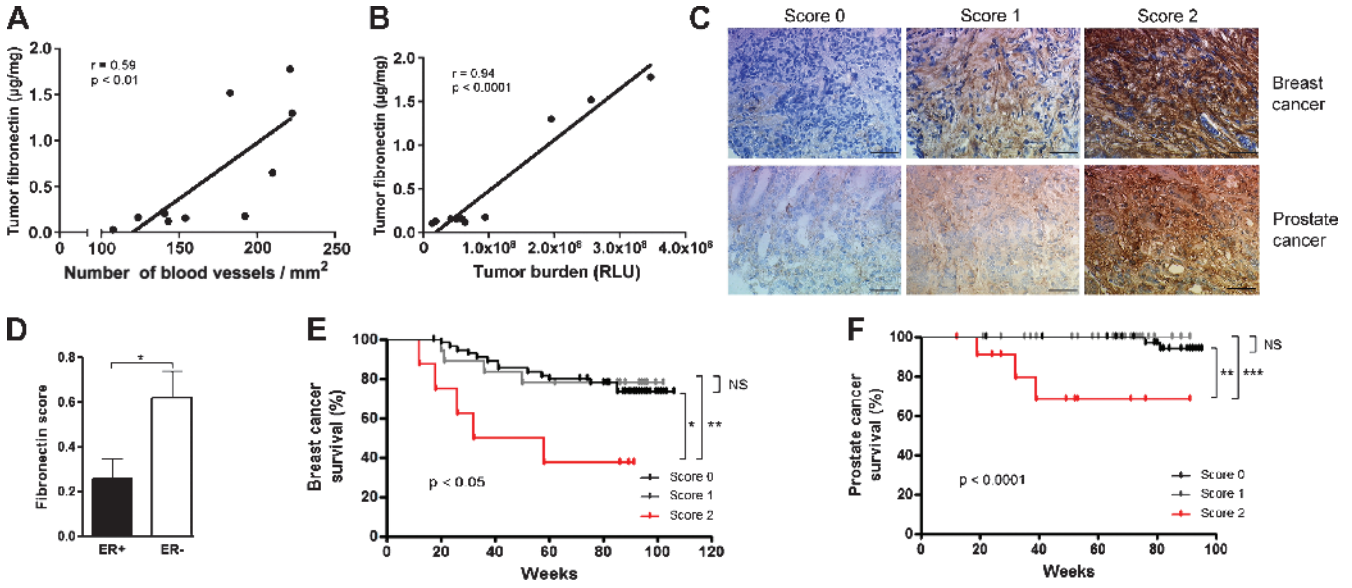

Figure 6. Implications and relevance in human cancer. (A) Fibronectin content in tumors correlates with blood vessel numbers in the whole group including CT, Alb-cKO, and Mx-cKO mice ($N = 4$ CT, 3 Alb-cKO, and 3 Mx-cKO). Fibronectin content was determined by ELISA and corrected to protein content. (B) Fibronectin content in tumors determined by ELISA correlates with bioluminescence signal in the same groups as A. (C) Grading of staining intensity for breast and prostate cancer tissue arrays. (D) Fibronectin staining intensity is stronger in tumors that are ER negative (ER− = 42, ER+ = 39 samples). Kaplan-Meier survival curves for different fibronectin staining intensities in (E) breast cancer ($N = 81$) and (F) prostate cancer ($N = 89$). *$P < .05$, **$P < .01$, ***$P < .001$.

or HER2 status. In a Cox regression model including fibronectin staining, T, N, ER, PR, and HER2 status, the model was significant ($P < .05$). A stepwise forward variable selection, however, identified ER status as the only significant predictive factor, while fibronectin barely failed significance at $P = .06$.

To determine whether other tumors showed a similar relationship, we investigated the relationship between fibronectin staining intensity in tumor and the 5-year risk of death in a cohort of 82 patients with localized prostate cancer. None of the patients without staining on a scale of 0 to 2 died (0/48), while 1 of 28 (4% of patients) with weak staining and 2 of 6 (33% of patients) with strong staining died (0.006). No relationship between fibronectin staining intensity and Gleason score, tumor stage, lymph node metastasis, or relapse was found, however.

On the basis of these encouraging results, we expanded the analysis to a second prostate array of patients who underwent radical

Table 1. Clinical and Histopathologic Characteristics of the Patients in the Breast Cancer Tissue Microarray.

Effect	Level	Number of Patients	Cancer-Specific Survival			Time to Local Recurrence			Time to Metastasis Formation		
			Global *P*	Events	HR with 95% CI	Global *P*	Events	HR with 95% CI	Global *P*	Events	HR with 95% CI
Age at diagnosis	≤50	20	.182	8	(Ref.)	.973	2	(Ref.)	.259	9	(Ref.)
	>50	61		15	0.56 (0.24-1.33)		6	0.97 (0.20-4.83)		21	1.56 (0.71-3.42)
T	1	40	.118	7	(Ref.)	.361	2	(Ref.)	**.001**	**8**	(Ref.)
	2	31		12	2.65 (1.04-6.74)		5	3.70 (0.72-19.16)		15	3.36 (1.42-7.97)
	3	8		4	1.99 (0.67-5.91		1	1.39 (0.17-11.64)		6	2.70 (1.08-6.72)
	4	2		0	–		0	–		1	1.58 (0.21-11.69)
N	0	46	.266	9	(Ref.)	.496	4	(Ref.)	**<.001**	**11**	(Ref.)
	1	18		9	2.85 (1.13-7.19)		4	3.02 (0.75-12.07)		7	1.88 (0.73-4.86)
	2	6		1	0.50 (0.67-3.75)		0	–		4	2.78 (0.93-8.25)
	3	10		4	1.77 (0.52-6.00)		0	–		7	2.11 (0.88-5.06)
	4	1		0	–		0	–		1	61.50 (3.84-985)
ER	Negative	42	**<.001**	19	(Ref.)	**.027**	7	(Ref.)	**.033**	19	(Ref.)
	Positive	39		4	0.18 (0.06-0.53)		1	0.13 (0.02-1.09)		11	0.45 (0.22-0.96)
PR	Negative	51	.396	16	(Ref.)	.436	6	(Ref.)	.133	22	(Ref.)
	Positive	30		7	0.68 (0.28-1.66)		2	0.56 (0.11-2.65)		8	0.54 (0.24-1.22)
HER2	Negative	63	.585	17	(Ref.)	.833	6	(Ref.)	.276	26	(Ref.)
	Positive	18		6	1.30 (0.51-3.29)		2	1.19 (0.24-5.89)		4	0.56 (0.20-1.61)
Fibronectin score	0	54	**.013**	13	(Ref.)	.6699	5	(Ref.)	.124	19	(Ref.)
	1	18		5	0.96 (0.31-2.93)		2	1.20 (0.23-6.20)		7	1.31 (0.55-3.11)
	2	9		5	4.61 (1.73-12.31)		1	1.43 (0.17-12.10)		4	1.71 (0.58-5.04)
Fibronectin score	0 + 1	72	**<.001**	17	(Ref.)	.706	7	(Ref.)	.259	26	(Ref.)
	2	9		6	4.56 (1.79-11.63)		1	1.50 (0.18-12.27)		4	1.83 (0.63-2.30)

T indicates tumor size; N, nodal status; HR, hazard ratio; CI, confidence interval; Ref., reference. Significant *P* values are **bolded**.

Table 2. Clinical and Histopathologic Characteristics of the Patients in the Second Prostate Tissue Microarray.

Effect	Level	Number of Patients	Cancer-Specific Survival			Time to Local Recurrence			Time to Metastasis Formation		
			Global *P*	Events	HR with 95% CI	Global *P*	Events	HR with 95% CI	Global *P*	Events	HR with 95% CI
PSA (ng/ml)	≤4	18	.168	0	(Ref.)	.196	3	(Ref.)	.335	1	(Ref.)
	4-10	33		2	2×10^5 (0 to $>10^{10}$)		11	2.70 (0.75-9.75		4	2.74 (0.30-24.73)
	>10	38		4	664 (0 to $>10^{10}$)		13	1.56 (0.67-3.61)		6	1.81 (0.47-7.04)
		89									
T	0	54	.053	2	(Ref.)	**<.001**	11	(Ref.)	**.001**	3	(Ref.)
	1	29		4	4.65 (0.84-25.6)		16	4.66 (2.10-10.35)		8	6.88 (1.81-26.14)
N	0	83	**.001**	4	(Ref.)	**<.001**	24	(Ref.)	**.002**	9	(Ref.)
	1	5		2	9.86 (1.79-54.45)		3	6.74 (1.98-22.90)		2	8.03 (1.70-37.96)
Gleason score	0-7a	70	**.004**	2	(Ref.)	**.004**	17	(Ref.)	**.003**	5	(Ref.)
	>7a	19		4	8.02 (1.47-43.84)		10	2.96 (1.36-6.48)		6	5.09 (1.55-16.67)
Resection	R0	71	**.007**	3	(Ref.)	**.001**	18	(Ref.)	**.015**	7	(Ref.)
	R1	18		3	7.27 (1.36-38.78)		9	3.68 (1.64-8.26)		4	4.29 (1.21-15.23)
Fibronectin score	0	41	**.031**	3	(Ref.)	.086	11	(Ref.)	**.004**	4	(Ref.)
	1	36		0	–		13	1.98 (0.85-4.63)		4	2.48 (0.56-10.99)
	2	12		3	3390 (0 to $>10^{10}$)		3	1.63 (0.49-5.47)		3	6.71 (1.72-26.08)
Fibronectin score	0 + 1	77	**<.001**	3	(Ref.)	.420	24	(Ref.)	**.001**	8	(Ref.)
	2	12		3	12.83 (2.46-66.92)		3	1.64 (0.49-5.49)		3	7.00 (1.77-27.64)

PSA indicates prostate-specific antigen; T, tumor size; N, nodal status; HR, hazard ratio; CI, confidence interval; Ref., reference. Significant *P* values are **bolded**.

prostatectomy with a median follow-up of 73 months. Eighty-nine biopsies could be evaluated for fibronectin staining. Forty-one samples showed no staining, 36 weak staining, and 12 strong staining (Figure 6*C* and Table 2). The presence of positive regional lymph nodes was higher in tumors with strong staining (0% without staining *vs* 20% with strong staining, $P < .01$). There was no relationship however between staining intensity and either prostate-specific antigen concentration, Gleason score, or tumor expansion (T) at diagnosis. Kaplan-Meier survival curves showed no difference between survival of patients with tumors either without or with weak staining, but cancer-specific survival of the relatively small group of patients with tumors with strong staining was diminished (Figure 6*F*). Indeed, a Cox regression model analysis that included T, N, Gleason score, and fibronectin staining intensity (none or weak *vs* strong) identified fibronectin staining as the only significant predictive factor ($P < .05$). The same was true of metastasis-free survival, while none of the examined parameters correlated with time to biochemical recurrence.

In summary, strong fibronectin staining intensity albeit a relatively rare event is associated with poor cancer-specific survival (Figure 6, *E* and *F*).

Discussion

The principal findings of our study are given as follows: 1) Deletion of circulating fibronectin results in decreased tumor growth. This is mediated by decreased fibronectin content resulting in lower VEGF concentrations, suppressed angiogenesis, as well as diminished proliferation and enhanced apoptosis. 2) The amount of tumor fibronectin seems to be prognostically relevant in human breast and prostate cancers. Thus, circulating fibronectin by affecting local fibronectin production contributes to tumor progression and prognosis.

Deletion of fibronectin in the circulation and in the bone marrow did not affect cancer cell homing to the bone marrow or the number of metastatic lesions in our model. This is in contrast to findings by Malik et al. in a lung cancer model [11], where deletion of fibronectin resulted in a decrease in the number of lung lesions. This was attributed to fibronectin-containing clots that protect cancer cells in the circulation and facilitate extravasation. The difference between both models could be the presence of sinusoids in the bone marrow but not in the lungs. These sinusoids allow for easy extravasation similar to the case with liver metastases [11,39]. Furthermore, our findings suggest that in the absence of circulating fibronectin bone marrow fibronectin content does not enhance the establishment potential of circulating cancer cells in the bone marrow, despite published reports that local fibronectin provides a permissive environment for lung cancer metastasis [15].

Tumor growth depends on the formation of blood vessels. During the early steps of angiogenesis, endothelial cells modify the surrounding extracellular matrix and produce fibronectin [25,40]. Endothelial cells from Mx-cKO showed reduced proliferation that partially normalized by addition of exogenous fibronectin. This is consistent with *in vitro* work showing that soluble fibronectin is integrated in the matrix in a cell-dependent manner [41] and confirmed by our results showing incorporation of injected labeled fibronectin in tumor tissue. Our findings further suggest that endothelial fibronectin can be mostly replaced by circulating fibronectin.

A key step in angiogenesis is vessel maturation evidenced by the recruitment of pericytes [42,43]. Endothelial and/or pericyte fibronectin could promote maturation by supporting tube stabilization [30,44] and recruitment of mesenchymal cells to sites of vascular remodeling [34]. In line with these data, our findings suggest that fibronectin modulates recruitment and differentiation of pericytes. Fibronectin isoforms EDA and EDB [18,19] are expressed in newly formed blood vessels in tumors [45–47]. Even though the absence of either one did not affect tumor neovascularization [45], the simultaneous absence of both was associated with defects in early vessel formation and diminished maturation in transgenic mice [48]. These findings are extended by our results showing a more pronounced decrease in vessel maturation in Mx-cKO compared to Alb-cKO tumors and attributing this effect to loss of endothelial and pericyte fibronectin production. The decrease in vessel maturation in Alb-cKO tumors however additionally implicates circulating fibronectin in pericyte recruitment, possibly because of the ability of circulating fibronectin to increase its production locally through a positive feedback loop as shown. The effects of circulating fibronectin may thus partially explain the incomplete effects seen with use of angiogenesis inhibitors [49].

The correlation between the amount of fibronectin in the tumor and both blood vessels and cancer growth is a central result of our study. Our data demonstrate that the amount of fibronectin within the tumor controls VEGF content and modulates VEGF-mediated signaling and, hence, blood vessel formation and subsequent tumor growth. Since it might be difficult to quantify fibronectin in samples received by pathologists, we examined whether fibronectin staining provides useful information about tumor growth based on suggestions in a prior study [50]. Indeed, staining intensity correlated with tumor growth in our model and with death in patients with breast and prostate cancers. In prostate cancer, death was best predicted by fibronectin staining intensity, which could be used to identify patients who require more aggressive therapy.

In summary, we show that circulating fibronectin plays a critical role in tumor growth. Circulating, cancer cell and endothelial/pericyte fibronectin cooperate to induce blood vessel formation and maturation and, hence, tumor growth by modifying VEGF content in tumors and potentiating VEGF-mediated signaling and effects. As a consequence, tumor fibronectin correlates with tumor growth in mice and is predictive of death in patients with breast and prostate cancers. This work thus expands on the traditional cell- and microenvironment-centered view of cancer growth and opens up new perspectives on the understanding of cancer growth.

Acknowledgments

We thank Reinhard Fässler for his invaluable input and Stefan Meuer for his continued support. We thank Jane Sottile and Dario Neri for reagents. We acknowledge the use of the Nikon Imaging Center at the University of Heidelberg.

References

[1] Levental KR, Yu H, Kass L, Lakins JN, Egeblad M, Erler JT, Fong SF, Csiszar K, Giaccia A, Weninger W, et al. (2009). Matrix crosslinking forces tumor progression by enhancing integrin signaling. *Cell* **139**, 891–906.

[2] Oskarsson T, Acharyya S, Zhang XH, Vanharanta S, Tavazoie SF, Morris PG, Downey RJ, Manova-Todorova K, Brogi E, and Massague J (2011). Breast cancer cells produce tenascin C as a metastatic niche component to colonize the lungs. *Nat Med* **17**, 867–874.

[3] Manabe R, Ohe N, and Sekiguchi K (1999). Alternatively spliced EDA segment regulates fibronectin-dependent cell cycle progression and mitogenic signal transduction. *J Biol Chem* **274**, 5919–5924.

[4] Ohnishi T, Hiraga S, Izumoto S, Matsumura H, Kanemura Y, Arita N, and Hayakawa T (1998). Role of fibronectin-stimulated tumor cell migration in glioma invasion *in vivo*: clinical significance of fibronectin and fibronectin receptor expressed in human glioma tissues. *Clin Exp Metastasis* **16**, 729–741.

[5] Sakai T, Johnson KJ, Murozono M, Sakai K, Magnuson MA, Wieloch T, Cronberg T, Isshiki A, Erickson HP, and Fassler R (2001). Plasma fibronectin supports neuronal survival and reduces brain injury following transient focal cerebral ischemia but is not essential for skin-wound healing and hemostasis. *Nat Med* **7**, 324–330.

[6] Moursi AM, Damsky CH, Lull J, Zimmerman D, Doty SB, Aota S, and Globus RK (1996). Fibronectin regulates calvarial osteoblast differentiation. *J Cell Sci* **109**(pt 6), 1369–1380.

[7] Johansson S, Svineng G, Wennerberg K, Armulik A, and Lohikangas L (1997). Fibronectin-integrin interactions. *Front Biosci* **2**, d126–d146.

[8] Sottile J and Hocking DC (2002). Fibronectin polymerization regulates the composition and stability of extracellular matrix fibrils and cell-matrix adhesions. *Mol Biol Cell* **13**, 3546–3559.

[9] Goerges AL and Nugent MA (2004). pH regulates vascular endothelial growth factor binding to fibronectin: a mechanism for control of extracellular matrix storage and release. *J Biol Chem* **279**, 2307–2315.

[10] Bentmann A, Kawelke N, Moss D, Zentgraf H, Bala Y, Berger I, Gasser JA, and Nakchbandi IA (2010). Circulating fibronectin affects bone matrix, whereas osteoblast fibronectin modulates osteoblast function. *J Bone Miner Res* **25**, 706–715.

[11] Malik G, Knowles LM, Dhir R, Xu S, Yang S, Ruoslahti E, and Pilch J (2010). Plasma fibronectin promotes lung metastasis by contributions to fibrin clots and tumor cell invasion. *Cancer Res* **70**, 4327–4334.

[12] Benoy IH, Elst H, Philips M, Wuyts H, Van Dam P, Scharpe S, Van Marck E, Vermeulen PB, and Dirix LY (2006). Real-time RT-PCR detection of disseminated tumour cells in bone marrow has superior prognostic significance in comparison with circulating tumour cells in patients with breast cancer. *Br J Cancer* **94**, 672–680.

[13] Morgan TM, Lange PH, Porter MP, Lin DW, Ellis WJ, Gallaher IS, and Vessella RL (2009). Disseminated tumor cells in prostate cancer patients after radical prostatectomy and without evidence of disease predicts biochemical recurrence. *Clin Cancer Res* **15**, 677–683.

[14] Shiozawa Y, Pedersen EA, Havens AM, Jung Y, Mishra A, Joseph J, Kim JK, Patel LR, Ying C, Ziegler AM, et al. (2011). Human prostate cancer metastases target the hematopoietic stem cell niche to establish footholds in mouse bone marrow. *J Clin Invest* **121**, 1298–1312.

[15] Kaplan RN, Riba RD, Zacharoulis S, Bramley AH, Vincent L, Costa C, MacDonald DD, Jin DK, Shido K, Kerns SA, et al. (2005). VEGFR1-positive haematopoietic bone marrow progenitors initiate the pre-metastatic niche. *Nature* **438**, 820–827.

[16] Segre JA, Nemhauser JL, Taylor BA, Nadeau JH, and Lander ES (1995). Positional cloning of the nude locus: genetic, physical, and transcription maps of the region and mutations in the mouse and rat. *Genomics* **28**, 549–559.

[17] Constien R, Forde A, Liliensiek B, Grone HJ, Nawroth P, Hammerling G, and Arnold B (2001). Characterization of a novel EGFP reporter mouse to monitor Cre recombination as demonstrated by a Tie2 Cre mouse line. *Genesis* **30**, 36–44.

[18] Kawelke N, Bentmann A, Hackl N, Hager HD, Feick P, Geursen A, Singer MV, and Nakchbandi IA (2008). Isoform of fibronectin mediates bone loss in patients with primary biliary cirrhosis by suppressing bone formation. *J Bone Miner Res* **23**, 1278–1286.

[19] Hackl NJ, Bersch C, Feick P, Antoni C, Franke A, Singer MV, and Nakchbandi IA (2010). Circulating fibronectin isoforms predict the degree of fibrosis in chronic hepatitis C. *Scand J Gastroenterol* **45**, 349–356.

[20] Kawelke N, Vasel M, Sens C, von Au A, Dooley S, and Nakchbandi IA (2011). Fibronectin protects from excessive liver fibrosis by modulating the availability of and responsiveness of stellate cells to active TGF-β. *PLoS One* **6**, e28181.

[21] Havens AM, Pedersen EA, Shiozawa Y, Ying C, Jung Y, Sun Y, Neeley C, Wang J, Mehra R, Keller ET, et al. (2008). An *in vivo* mouse model for human prostate cancer metastasis. *Neoplasia* **10**, 371–380.

[22] Wetterwald A, van der Pluijm G, Que I, Sijmons B, Buijs J, Karperien M, Lowik CW, Gautschi E, Thalmann GN, and Cecchini MG (2002). Optical imaging of cancer metastasis to bone marrow: a mouse model of minimal residual disease. *Am J Pathol* **160**, 1143–1153.

[23] Dong QG, Bernasconi S, Lostaglio S, De Calmanovici RW, Martin-Padura I, Breviario F, Garlanda C, Ramponi S, Mantovani A, and Vecchi A (1997). A general strategy for isolation of endothelial cells from murine tissues. Characterization of two endothelial cell lines from the murine lung and subcutaneous sponge implants. *Arterioscler Thromb Vasc Biol* **17**, 1599–1604.

[24] Allport JR and Weissleder R (2003). Murine Lewis lung carcinoma-derived endothelium expresses markers of endothelial activation and requires tumor-specific extracellular matrix *in vitro*. *Neoplasia* **5**, 205–217.

[25] Zhou X, Rowe RG, Hiraoka N, George JP, Wirtz D, Mosher DF, Virtanen I, Chernousov MA, and Weiss SJ (2008). Fibronectin fibrillogenesis regulates three-dimensional neovessel formation. *Genes Dev* **22**, 1231–1243.

[26] Mitchell TS, Bradley J, Robinson GS, Shima DT, and Ng YS (2008). RGS5 expression is a quantitative measure of pericyte coverage of blood vessels. *Angiogenesis* **11**, 141–151.

[27] Muller WA, Ratti CM, McDonnell SL, and Cohn ZA (1989). A human endothelial cell-restricted, externally disposed plasmalemmal protein enriched in intercellular junctions. *J Exp Med* **170**, 399–414.

[28] Stan RV, Kubitza M, and Palade GE (1999). PV-1 is a component of the fenestral and stomatal diaphragms in fenestrated endothelia. *Proc Natl Acad Sci USA* **96**, 13203–13207.

[29] Sacchetti B, Funari A, Michienzi S, Di Cesare S, Piersanti S, Saggio I, Tagliafico E, Ferrari S, Robey PG, Riminucci M, et al. (2007). Self-renewing osteoprogenitors in bone marrow sinusoids can organize a hematopoietic microenvironment. *Cell* **131**, 324–336.

[30] Stratman AN, Malotte KM, Mahan RD, Davis MJ, and Davis GE (2009). Pericyte recruitment during vasculogenic tube assembly stimulates endothelial basement membrane matrix formation. *Blood* **114**, 5091–5101.

[31] Williams CM, Engler AJ, Slone RD, Galante LL, and Schwarzbauer JE (2008). Fibronectin expression modulates mammary epithelial cell proliferation during acinar differentiation. *Cancer Res* **68**, 3185–3192.

[32] Nicosia RF, Bonanno E, and Smith M (1993). Fibronectin promotes the elongation of microvessels during angiogenesis *in vitro*. *J Cell Physiol* **154**, 654–661.

[33] Han SW and Roman J (2006). Fibronectin induces cell proliferation and inhibits apoptosis in human bronchial epithelial cells: pro-oncogenic effects mediated by PI3-kinase and NF-κB. *Oncogene* **25**, 4341–4349.

[34] Veevers-Lowe J, Ball SG, Shuttleworth A, and Kielty CM (2011). Mesenchymal stem cell migration is regulated by fibronectin through α5β1-integrin-mediated activation of PDGFR-β and potentiation of growth factor signals. *J Cell Sci* **124**, 1288–1300.

[35] Wijelath ES, Rahman S, Namekata M, Murray J, Nishimura T, Mostafavi-Pour Z, Patel Y, Suda Y, Humphries MJ, and Sobel M (2006). Heparin-II domain of fibronectin is a vascular endothelial growth factor-binding domain: enhancement of VEGF biological activity by a singular growth factor/matrix protein synergism. *Circ Res* **99**, 853–860.

[36] Miyamoto S, Teramoto H, Gutkind JS, and Yamada KM (1996). Integrins can collaborate with growth factors for phosphorylation of receptor tyrosine kinases and MAP kinase activation: roles of integrin aggregation and occupancy of receptors. *J Cell Biol* **135**, 1633–1642.

[37] Cabon L, Galan-Malo P, Bouharrour A, Delavallee L, Brunelle-Navas MN, Lorenzo HK, Gross A, and Susin SA (2011). BID regulates AIF-mediated caspase-independent necroptosis by promoting BAX activation. *Cell Death Differ* **19**, 245–256.

[38] Zhang Z, Vuori K, Reed JC, and Ruoslahti E (1995). The α5β1 integrin supports survival of cells on fibronectin and up-regulates Bcl-2 expression. *Proc Natl Acad Sci USA* **92**, 6161–6165.

[39] Braet F and Wisse E (2002). Structural and functional aspects of liver sinusoidal endothelial cell fenestrae: a review. *Comp Hepatol* **1**, 1.

[40] Risau W and Lemmon V (1988). Changes in the vascular extracellular matrix during embryonic vasculogenesis and angiogenesis. *Dev Biol* **125**, 441–450.

[41] McKeown-Longo PJ and Mosher DF (1985). Interaction of the 70,000-mol-wt amino-terminal fragment of fibronectin with the matrix-assembly receptor of fibroblasts. *J Cell Biol* **100**, 364–374.

[42] Rangdaeng S and Truong LD (1991). Comparative immunohistochemical staining for desmin and muscle-specific actin. A study of 576 cases. *Am J Clin Pathol* **96**, 32–45.

[43] Tallquist MD, French WJ, and Soriano P (2003). Additive effects of PDGF receptor β signaling pathways in vascular smooth muscle cell development. *PLoS Biol* **1**, E52.

[44] George EL, Baldwin HS, and Hynes RO (1997). Fibronectins are essential for heart and blood vessel morphogenesis but are dispensable for initial specification of precursor cells. *Blood* **90**, 3073–3081.

[45] Astrof S, Crowley D, George EL, Fukuda T, Sekiguchi K, Hanahan D, and Hynes RO (2004). Direct test of potential roles of EIIIA and EIIIB alternatively spliced segments of fibronectin in physiological and tumor angiogenesis. *Mol Cell Biol* **24**, 8662–8670.

[46] Palumbo A, Hauler F, Dziunycz P, Schwager K, Soltermann A, Pretto F, Alonso C, Hofbauer GF, Boyle RW, and Neri D (2011). A chemically modified antibody mediates complete eradication of tumours by selective disruption of tumour blood vessels. *Br J Cancer* **104**, 1106–1115.

[47] Villa A, Trachsel E, Kaspar M, Schliemann C, Sommavilla R, Rybak JN, Rosli C, Borsi L, and Neri D (2008). A high-affinity human monoclonal antibody specific to the alternatively spliced EDA domain of fibronectin efficiently targets tumor neo-vasculature *in vivo*. *Int J Cancer* **122**, 2405–2413.

[48] Astrof S, Crowley D, and Hynes RO (2007). Multiple cardiovascular defects caused by the absence of alternatively spliced segments of fibronectin. *Dev Biol* **311**, 11–24.

[49] Carmeliet P and Jain RK (2011). Molecular mechanisms and clinical applications of angiogenesis. *Nature* **473**, 298–307.

[50] Yao ES, Zhang H, Chen YY, Lee B, Chew K, Moore D, and Park C (2007). Increased β1 integrin is associated with decreased survival in invasive breast cancer. *Cancer Res* **67**, 659–664.

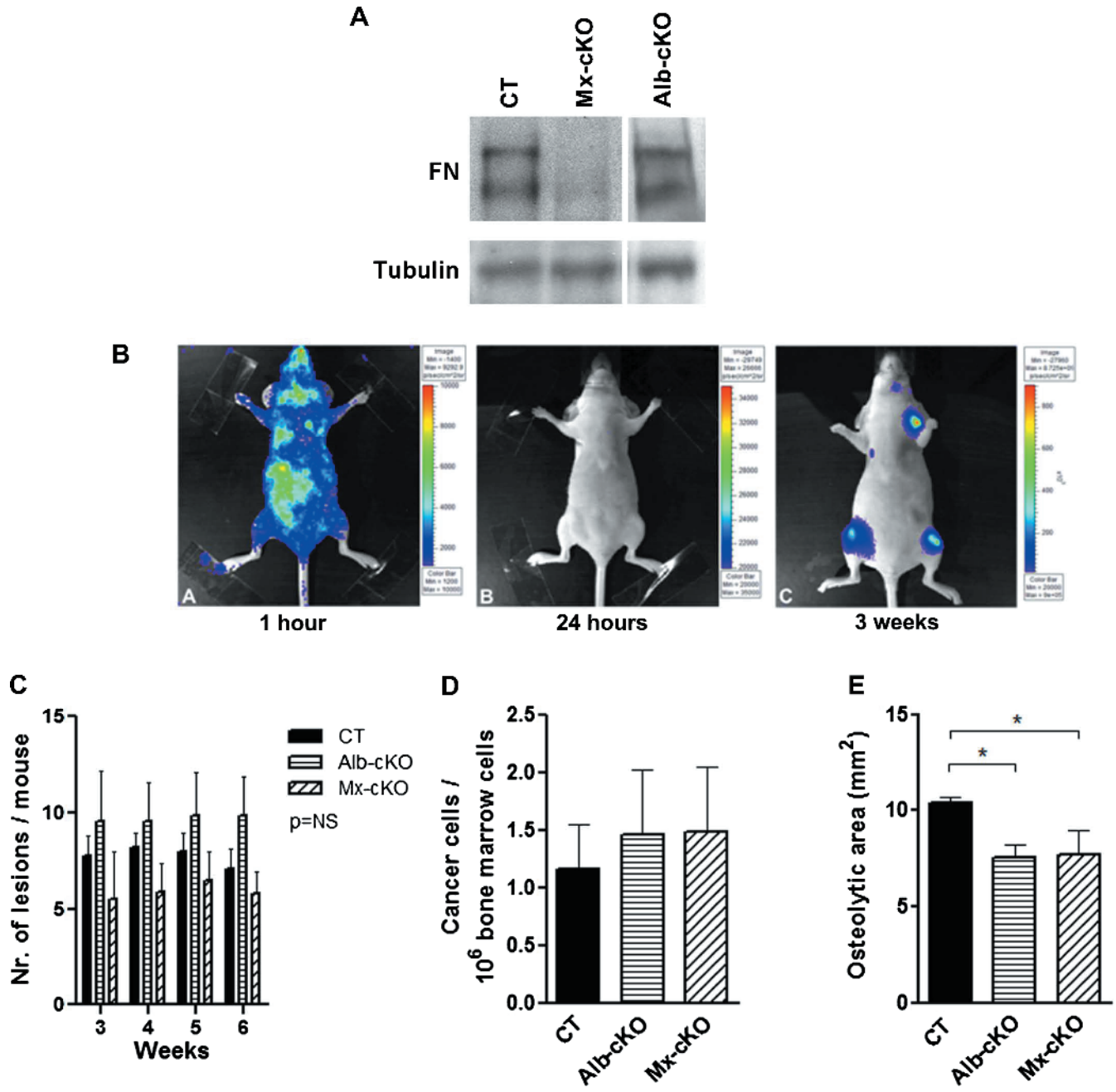

Figure W1. (A) Western blot of bone marrow lysate confirms decreased fibronectin content (FN) in Mx-cKO and normal content in Alb-cKO. Bone marrow was flushed with 100 μl of protein lysis buffer/femur. (B) Bioluminescence signal after intracardiac injection of MDA-MB-231/B+: 1 hour after intracardiac injection, a very weak signal can be detected (embedded A), which is gone by 24 hours after injection (embedded B). Lesions are detected by 3 weeks after injection (embedded C). To measure the bioluminescence signal, mice were injected with 150 mg/kg luciferin exactly 5 minutes before starting measurements. (C) Intracardiac injection of MDA-MB-231 in Alb- and Mx-cKO mice results in a similar number of lesions per mouse as determined by BLI. The *x*-axis represents weeks since intracardiac injection (N = 11-12/group). (D) Homing of cancer cells to the bone marrow was not affected by the deletion of circulating fibronectin and/or fibronectin in the bone marrow, as determined by qPCR. Cancer cells (10^5) were injected intracardially, and 24 hours later, DNA was extracted and examined by qPCR for human alu. Results are adjusted to murine bone marrow (N = 6/group). (E) Intratibial injection is associated with a decrease in growth in both Alb- and Mx-cKO. The results of bioluminescence signal measurements are shown in Figure 1*F*. The decrease in the area of osteolysis at the end of the experiment at day 40 after intratibial injection is shown here (N = 9-11/group). *$P < .05$.

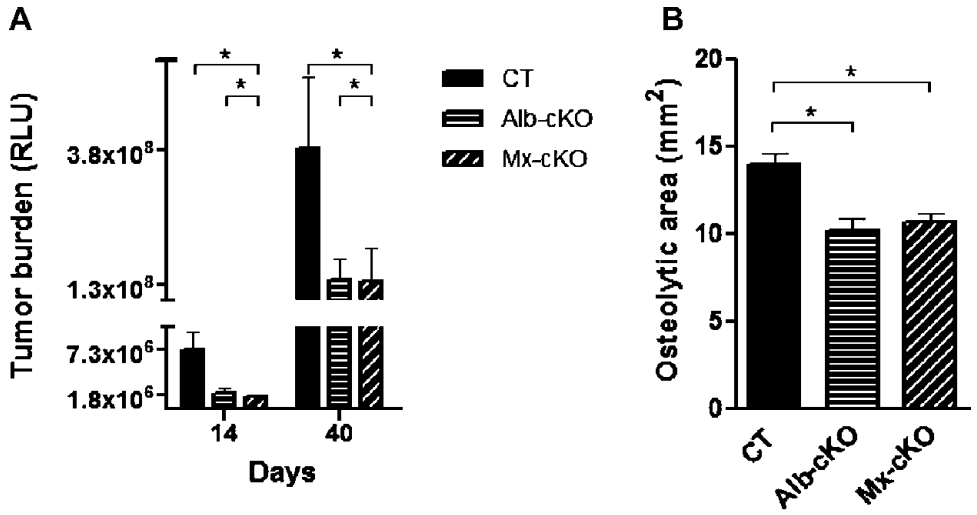

Figure W2. Findings in a model of prostate cancer. Tumor cells of the line PC3Mpro4/luc+ were injected intratibially in male mice, and bioluminescence signal was examined at the time points shown on A. (A) Decreased growth by bioluminescence signal ($N = 12$/group). (B) Area of osteolysis was diminished at the time of death 40 days after intratibial injection.

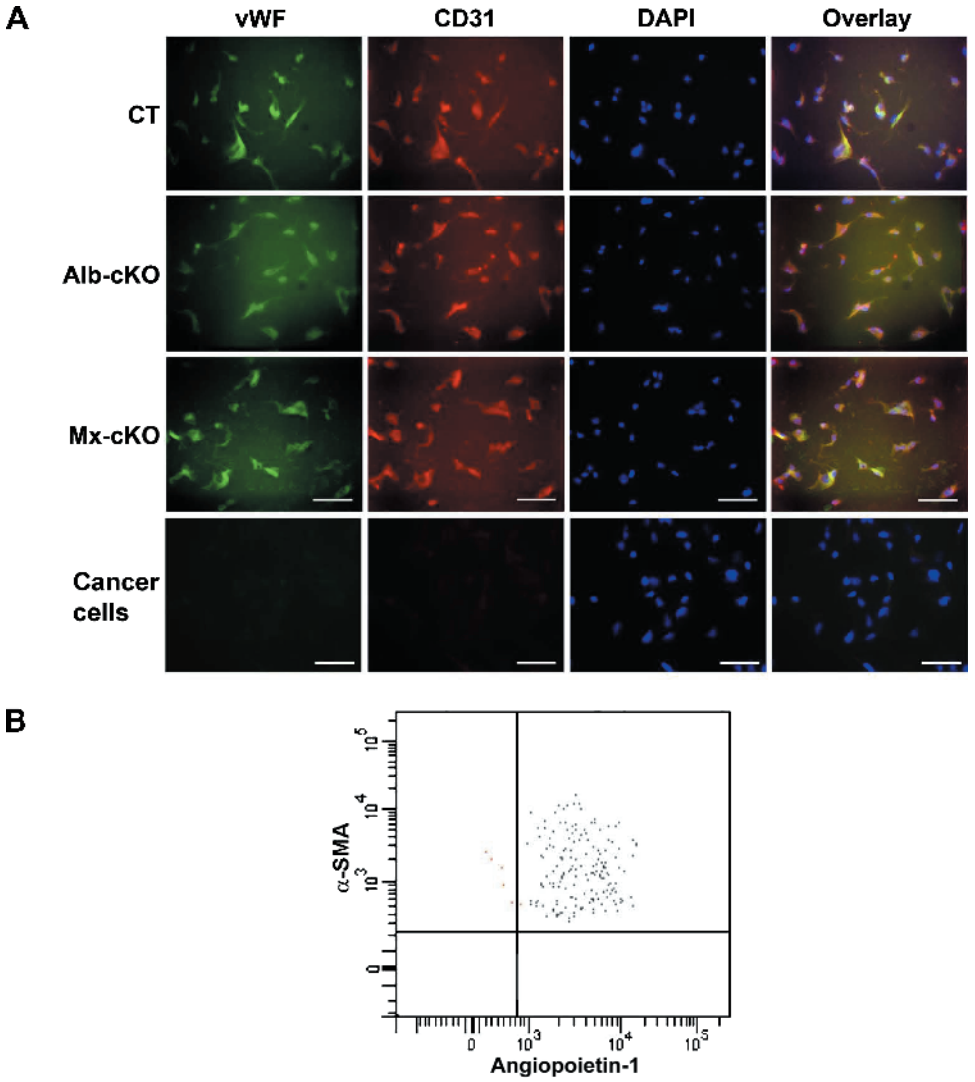

Figure W3. Confirmation of identity of isolated endothelial cells and pericytes. (A) Endothelial cells isolated using CD31-coated Dynabeads stained positive for both vWF and CD31. Nuclei were stained with 4',6-diamidino-2-phenylindole (DAPI). Cancer cells did not show any staining with either endothelial cell markers. Bars represent 50 μm. (B) Pericytes isolated by sorting stained positive for both angiopoietin-1 and α-SMA by flow cytometry.

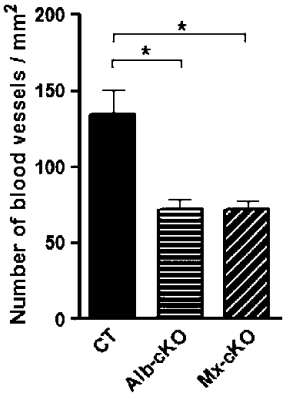

Figure W4. Angiogenesis in a prostate cancer model. Tumor cells of the line PC3Mpro4/luc+ were injected intratibially in male mice. Forty days after injection, mice were killed and tumors were examined using CD31 staining. There was a significant decrease in blood vessel numbers in Alb-cKO and Mx-cKO tumors, but no difference between Alb- and Mx-cKO tumors ($N = 4$/group). *$P < .05$.

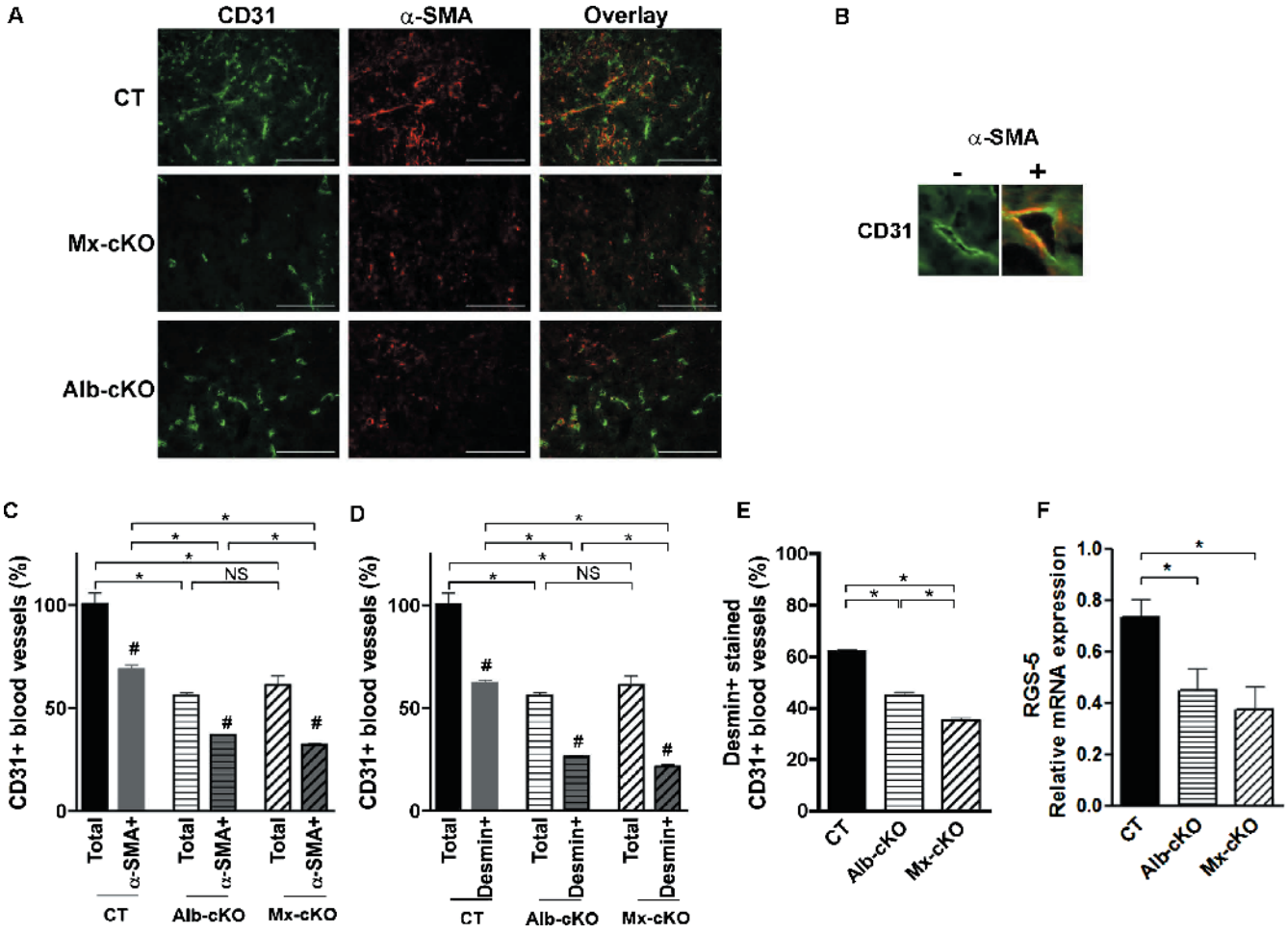

Figure W5. Effects of fibronectin on vessel maturation. (A) CD31+ blood vessels were additionally stained with α-SMA. Bars represent 200 μm. (B) A detailed view of a blood vessel co-stained with CD31 and α-SMA. The quantification is shown in Figure 3*E* and in C. (C) CD31+ blood vessel number was decreased in both cKO models to almost the same degree compared to CT (total). In addition, there was a decrease in double positive CD31+ α-SMA+ blood vessels in both cKOs, but their percentage was higher in Alb-cKO compared to Mx-cKO. The number of blood vessels corrected to the area in CT tumors was set at 100% to allow for comparison of relative changes between the groups. $^{\#}P < .05$ for α-SMA+ *versus* total in each group ($N = 3, 3, 6$ mice, four sections/mouse). (D) This graph is similar to C except that it shows the data for desmin staining instead of α-SMA. The number of blood vessels corrected to the area in CT tumors was set at 100% to allow for comparison of relative changes between the groups. $^{\#}P < .05$ for desmin+ *versus* total in each group. N as in C. (E) The decrease in the percentage of desmin+ blood vessels was more pronounced in Mx- than in Alb-cKO tumors. For the purpose of this graph, CT, Alb-cKO, and Mx-cKO CD31+ vessels were set at 100%. This graph is similar to Figure 3*E* except that it shows the data for desmin staining instead of α-SMA. N as in C. (F) Relative mRNA expression of the pericyte marker RGS5 was diminished in both cKOs ($N = 7$ CT, 4 Alb-cKO, and 5 Mx-cKO). $^{*}P < .05$, $^{**}P < .01$.

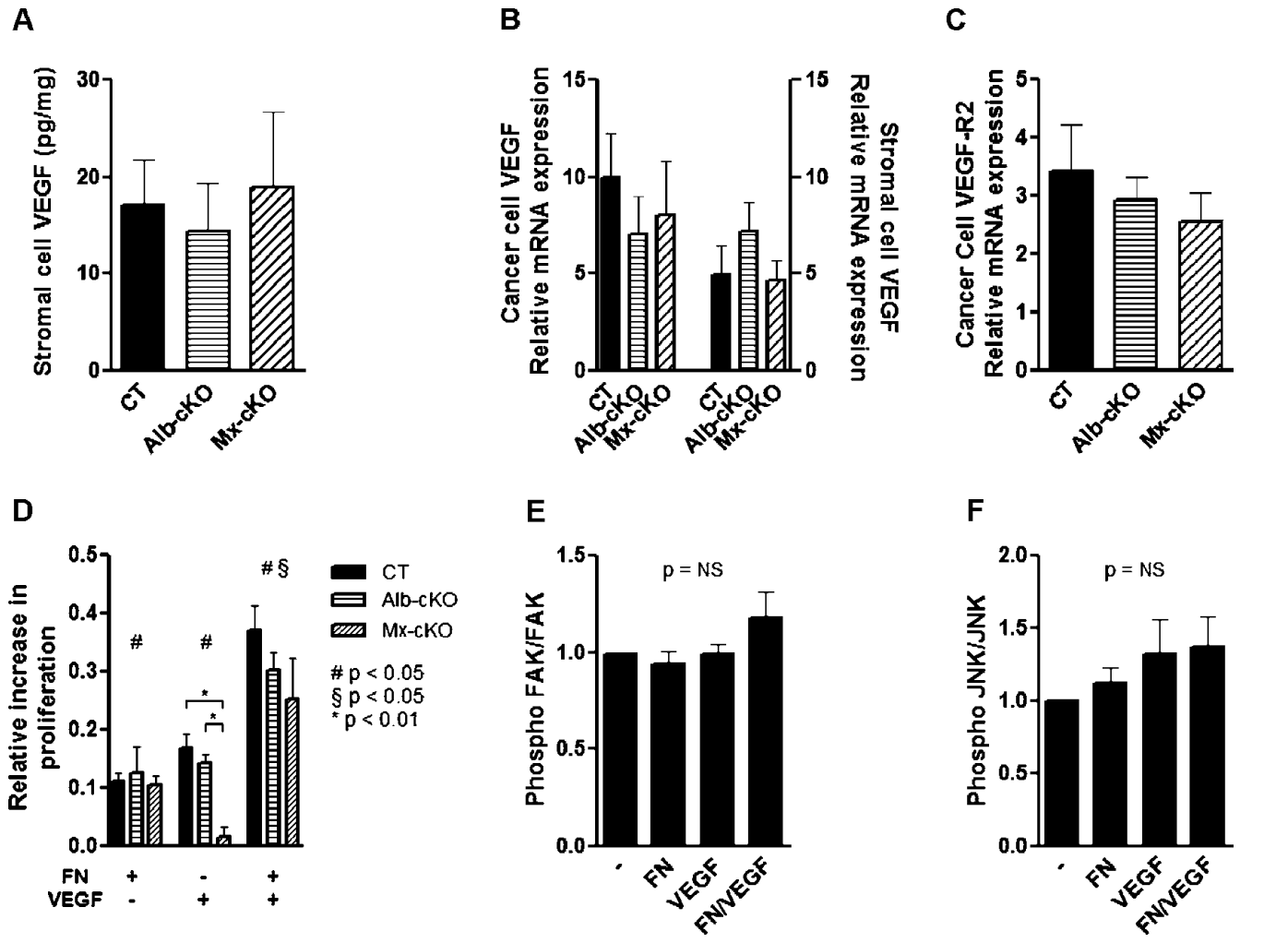

Figure W6. Changes in VEGF, VEGFR-2, and signaling *in vivo* and *in vitro*. (A) Murine VEGF originating from stromal cells was not affected in cKO tumors (measured using murine-specific ELISA), while cancer cell (human) VEGF was (shown in Figure 4*A*; $N = 4$-6/group). (B) Neither cancer cell nor stromal VEGF mRNA differed between CT and cKO tumors ($N = 4$/group). (C) Cancer cell (human) VEGFR-2 mRNA expression was not affected in cKO tumors, but murine VEGFR-2 (shown in Figure 4*D*) was ($N = 4$/group). (D) Cell proliferation was significantly increased when endothelial cells were treated with either fibronectin or VEGF compared to untreated cells, except for Mx-cKO endothelial cells, which failed to proliferate in response to VEGF alone. The addition of both simultaneously resulted in a more pronounced increase in proliferation in the three groups; # denotes significant change compared to baseline proliferation; § denotes significant increase compared to either fibronectin (FN) or VEGF alone ($N = 3$ experiments with three to five replicates/condition per experiment. (E and F) Fibronectin, VEGF, or the combination of both does not affect FAK (E) or JNK (F) phosphorylation in tumor endothelial cells. The data are the average of four experiments with three to five replicates/condition per experiment. Equal amounts of protein as measured by BCA were loaded. The Western blot is shown in Figure 4*G*.

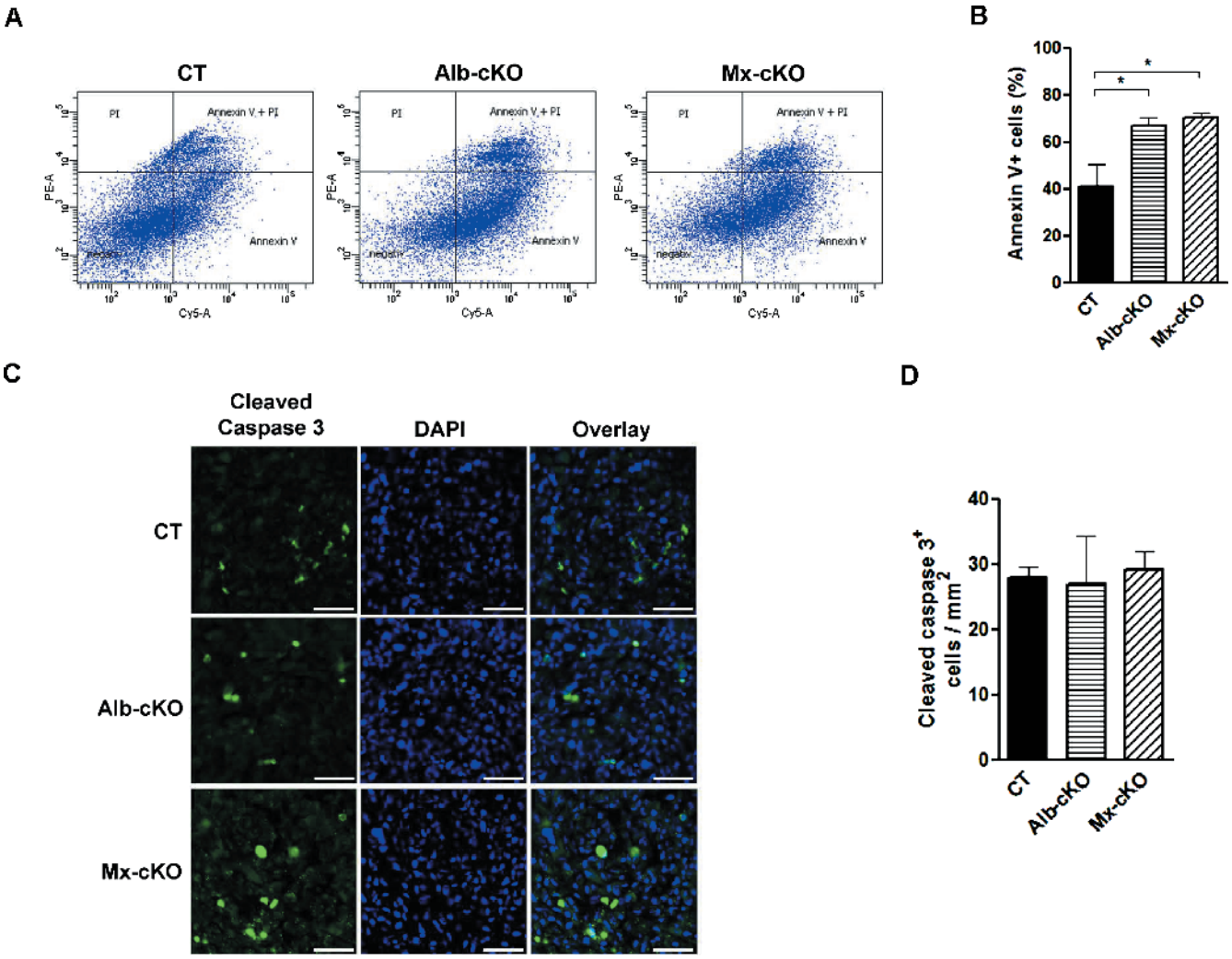

Figure W7. Effects of fibronectin on apoptosis. (A) Apoptosis in tumor was determined by digesting tumor tissue followed by staining for AV and PI. (B) The number of tumor cells stained positive with AV (AV+/PI+ and AV+/PI−) is increased in Mx-cKO and Alb-cKO tumors (N = 3/group). (C) Cleaved caspase-3 was not affected in Mx- and Alb-cKO tumors compared to CT. Bars represent 100 μm. (D) Quantification confirms absence of a difference (N = 6 CT, 3 Alb-cKO, and 3 Mx-cKO).

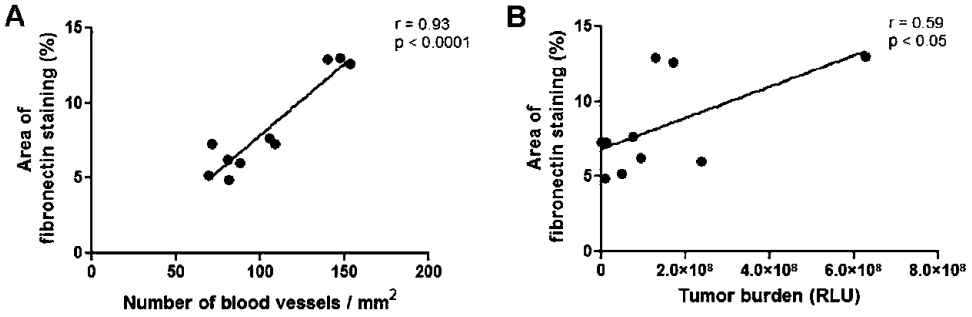

Figure W8. Correlations between fibronectin staining in intratibial MDA-MB-231b/luc+ tumors and blood vessel numbers or bioluminescence signal. (A) Area of fibronectin staining correlates with blood vessel numbers (N = 4 CT, 3 Alb-cKO, and 3 Mx-cKO). (B) Area of fibronectin staining correlates with bioluminescence signal in the same groups as A.